Strål
säkerhets
myndigheten
Swedish Radiation Safety Authority

Research

Cladding tube rupture under LOCA: Data and models for rupture opening size

2021:05

Authors: Lars Olof Jernkvist,
Quantum Technologies AB Uppsala Science Park
Report number: 2021:05
ISSN: 2000-0456
Available at: www.ssm.se

SSM perspective

Background

The Swedish Radiation Safety Authority (SSM) follows the research on fuel performance closely. One aspect that is currently being studied in several research projects is the risk of release of fragmented fuel into the primary coolant in case of an accident. This risk depends on complex conditions were one is the possibility and size of a rupture of the fuel rod cladding tube.

The work presented in this report is part of a larger endeavour to update the computer codes that SSM disposes of through Quantum Technologies AB. The work is a direct continuation of the development of cladding rupture criteria and fuel fragmentation models in previous projects. The present report analyses test results and deduces a model that can be used to predict fuel cladding burst opening sizes.

Results

In this project, cladding ruptures that have occurred in tests with simulated loss-of-coolant accident (LOCA) conditions are analysed regarding their dimensions and based on that an empirical model is proposed. In the analysis of test data, the most influential parameters are identified and their influence in the model considered. It is also concluded that there are several phenomena that affects the rupture dimensions and some are not easy to consider in computational analyses.

Relevance

With this project, SSM has gained insight into which parameters that are important when estimating the risk of dispersal of fuel from cladding tubes that rupture under typical LOCA conditions. SSM has also gained insight into how such a model can be used in a computer code and the uncertainties that it can include.

Understanding of fuel fragmentation and dispersal is used to further enhance the safety of nuclear fuel in accident conditions. With better understanding, more actual analysis can be performed and possible needs for revised limitations can be determined. Furthermore, this project is part of the international development work and enables active participation in international contexts

Need for further research

The continued development of models for analysing rupture behaviour in nuclear fuel is necessary. A continuation is to implement the model for burst dimensions and couple it to previously developed models for fuel fragmentation. More tests are also needed to understand the impact of stochastic phenomena and to further expand the database that the empirical model is built upon. On a longer time scale much research and development remains to fully understand the behaviour of high burnup fuel.

Project information

Contact person SSM: Anna Alvestav
Reference: SSM2018-4296 / 7030270-00

Strål
säkerhets
myndigheten
Swedish Radiation Safety Authority

Authors: Lars Olof Jernkvist
Quantum Technologies AB Uppsala Science Park

2021:05

Cladding tube rupture under LOCA: Data and models for rupture opening size

Date: February 2021
Report number: 2021:05 **ISSN:** 2000-0456
Available at www.stralsakerhetsmyndigheten.se

This report concerns a study which has been conducted for the Swedish Radiation Safety Authority, SSM. The conclusions and viewpoints presented in the report are those of the author/authors and do not necessarily coincide with those of the SSM.

Cladding tube rupture under LOCA: Data and models for rupture opening size

Lars Olof Jernkvist

January 8, 2021

Quantum Technologies AB
Uppsala Science Park
SE-751 83 Uppsala, Sweden

Cladding tube rupture under LOCA: Data and models for rupture opening size

Lars Olof Jernkvist

Quantum Technologies AB
Uppsala Science Park
SE-751 83 Uppsala, Sweden

Quantum Technologies Report: TR20-005V1
Project: SSM 2018-4296

Contents

Summary

In this report, empirical models are formulated, by which the rupture opening dimensions in zirconium alloy cladding tubes that fail by high-temperature ballooning and burst under typical light-water-reactor loss-of-coolant accident (LOCA) conditions can be estimated. The models, which are intended for implementation in computer programs for safety analysis, are needed for assessing the risk for ejection and dispersal of solid fuel pellet fragments into the primary reactor coolant, as a consequence of cladding tube failure.

A substantial database, comprising eight experiment series with totally 164 burst tests on single fuel rods under simulated LOCA conditions and six fuel assembly tests with altogether 121 failed rods, is compiled and analysed with regard to reported rupture opening dimensions. A considerable spread exists in these rupture opening data, not only between different test series, but also within test series where testing conditions are nominally identical for all samples. Possible causes to the spread are identified and discussed, and so are the most influential parameters for the rupture opening dimensions, differences between cladding materials, effects of irradiation and cladding hydrogen uptake under reactor operation.

Based on the analysis of available data, correlations are then formulated that relate fundamental rupture opening dimensions (area, axial length, circumferential width) to each other. The analysis shows that the circumferential width is the limiting dimensional parameter that will determine whether fuel pellet fragments of a given size may be ejected through the cladding breach. Subsequent work is therefore focussed on the width of the rupture opening, and a correlation is proposed, by which the width can be calculated from the as-fabricated dimensions of the cladding tube and the internal overpressure at time of burst. The correlation is formulated such that it may serve either as a best-estimate model or as a conservatively bounding model: the degree of conservatism (percentage of tests in the database bounded by the model) can be conveniently set by varying a single model parameter.

Available data suggest that there are differences between different types of zirconium base cladding materials regarding their rupture opening dimensions under LOCA, and that effects of irradiation and cladding corrosion may exist. However, the current database is insufficient to quantify these differences and effects. The proposed models are considered to be applicable to Zircaloy, M5 and ZIRLO cladding materials in un-irradiated as well as irradiated state.

Sammanfattning

I denna rapport utarbetas empiriska modeller för bestämning av ungefärliga dimensioner hos de brottöppningar som uppstår då kapslingsrör av zirconiumlegeringar brister vid hög temperatur under förhållanden typiska för haverisituationer med kylmedelsförlust (LOCA) i lättvattenreaktorer. Modellerna, vilka är avsedda att implementeras i beräkningsprogram för säkerhetsanalyser, är nödvändiga vid utvärdering av risken för att bränslekutsfragment läcker ut och sprids i reaktorns primärkylmedel till följd av kapslingsrörsskador.

En ansenlig databas, omfattande åtta experimentserier med totalt 164 sprängprov på enskilda provstavar under simulerade LOCA-förhållanden och sex prov på bränsleknippen med sammanlagt 121 brustna stavar, sammanställs och analyseras med avseende på rapporterade dimensioner hos brottöppningen.

Det finns en avsevärd spridning i denna data, inte enbart mellan olika provserier, utan även inom serier där provförhållandena är nominellt identiska för samtliga prov. Möjliga orsaker till denna spridning identifieras och diskuteras, liksom de mest betydelsefulla parametrarna för brottöppningens dimensioner samt effekter av bestrålning och kapslingens väteupptag under reaktordrift.

Från analysen av tillgängliga data formuleras korrelationer som relaterar fundamentala brottöppningsdimensioner (area, axiell längd och cirkumferentiell vidd) till varandra. Analysen visar att den cirkumferentiella vidden är den begränsande dimensionen, vilken kommer att avgöra om kutsfragment med viss storlek kan passera ut genom brottöppningen. Arbetet fokuseras därför fortsättningsvis på brottöppningens vidd, och en korrelation föreslås, varmed vidden kan beräknas från kapslingsrörets ursprungliga dimensioner och dess inre övertryck vid brottillfället. Korrelationen är utformad för att ge antingen en bästa skattning eller en konservativ skattning av brottöppningens vidd: graden av konservatism (procentandelen prov i databasen som begränsas av modellen) kan enkelt föreskrivas genom att variera en enda modellparameter.

Tillgängliga data antyder att olika typer av zirconiumbaserade kapslingsmaterial skiljer sig åt beträffande brottöppningens dimensioner under LOCA, och att det även kan finnas effekter av bestrålning och kapslingskorrosion. Emellertid är databasen i dagsläget otillräcklig för att kvantifiera dessa skillnader och effekter. De föreslagna modellerna bedöms vara tillämpliga för kapslingsmaterialen Zircaloy, M5 och ZIRLO, i såväl obestrålat som bestrålat tillstånd.

1 Introduction

1.1 Background

Loss-of-coolant accidents (LOCAs) are among the most important accident scenarios that light water reactor (LWR) safety systems and operational rules are designed to respond to [1]. With regard to fuel rod conditions, the most challenging scenarios for LWR LOCA lead to rapid heat-up of the cladding tube as the primary coolant is lost. With increasing temperature, the zirconium base cladding material loses its strength and becomes prone to creep and viscoplastic deformation. If the coolant pressure drops below the fuel rod internal gas pressure, creep and viscoplastic deformation may result in cladding tube distension ("ballooning") and ultimately, to cladding rupture [2].

Historically, safety analyses of postulated LOCA scenarios in LWR:s have been focussed on cladding tube ballooning and its potential to block coolant flow through the fuel assemblies and impair long-term core coolability. Until recently, prediction of cladding tube rupture has received less attention in these analyses. The consequences of cladding rupture are [2]:

- Immediate escape of the gas inventory in free volumes inside the fuel rod, e.g. gas in the pellet-cladding gap and rod plena, through the cladding breach;
- Ingress of steam into the pellet-cladding gap, leading to double-sided oxidation and hydriding of the failed cladding;
- Possible ejection of solid fuel pellet fragments through the cladding breach.

The last issue, which is the topic of this report, was brought into the limelight about fifteen years ago, when LOCA simulation tests on high-burnup LWR fuel rods gave evidence of ejection and dispersal of very fine fuel pellet fragments from the tested rods [3, 4]. The fuel fragment dispersal from these high-burnup (>65 MWd(kgU)$^{-1}$ pellet average burnup) rods was much more extensive than observed for rods with lower burnup in past LOCA simulation tests. Since the fuel dispersal under LOCA is a safety issue with regard to radiological consequences, criticality and coolability of the dispersed fuel, much research has been devoted to the phenomenon over the last fifteen years. Most of this research is summarized in a 2016 report [5], issued by the OECD Nuclear Energy Agency (NEA) Committee on the Safety of Nuclear Installations (CSNI). A similar report, including a review of relevant data from older (1970s-1990s) LOCA experiment series, was published in 2012 by the U.S. Nuclear Regulatory Commission (NRC) [6]. In the 2016 NEA/CSNI report, the following fundamental prerequisites for fuel pellet fragment dispersal under LWR LOCA were identified [5]:

1. Rupture of the cladding tube must occur;
2. Fuel pellet fragments must be smaller than the cladding rupture opening;
3. A certain distension of the cladding tube is needed for fuel pellet fragments to be axially mobile within the cladding.

The 2016 NEA/CSNI report also identified the computational models that are needed to assess the above prerequisites in fuel rod analysis programs used for LOCA. For the Swedish

Radiation Safety Authority (SSM), many of these modelling needs have been met by the development of appropriate models for the FRAPTRAN-1.5 program [7] in a series of research projects, carried out by Quantum Technologies (QT). More precisely, with regard to condition 1), available data and criteria for cladding rupture in LOCA conditions have been assessed [8], and suitable rupture criteria have been implemented in an extended QT-version of FRAPTRAN-1.5 and calibrated against experimental data [9].

To assess condition 2), models are needed for calculating the size distribution of fuel pellet fragments as well as the dimensions of the cladding rupture opening. Of particular importance is the observed tendency of high-burnup (>65 MWd(kgU)$^{-1}$ pellet average burnup) UO_2 fuel to disintegrate into very fine fuel fragments under LOCA. The phenomenon, commonly referred to as fuel powdering or fuel pulverization, is attributed to overpressurization and rupture of pores and grain boundary fission gas bubbles when the high-burnup fuel is overheated [10, 11]. The very fine (<0.2 mm) fuel fragments caused by this mechanism have a higher potential for axial relocation and subsequent dispersal into the coolant than the fairly large (>1 mm) fuel fragments that are typically observed in LOCA tests on low to medium burnup fuel. An empirical model for calculating the size distribution of fuel pellet fragments under LOCA conditions was developed and implemented in FRAPTRAN-QT-1.5 in 2015 [12], and mechanistic models for the same purpose were developed and implemented by QT in 2019 [13].

With regard to condition 3), a set of interconnected models for high-temperature creep deformation, solid-to-solid phase transformation and oxidation of zirconium alloy cladding tubes has been implemented in FRAPTRAN-QT-1.5 and calibrated against experimental data [9, 14]. These models provide more realistic calculations of the cladding deformation profile along the fuel rod, in comparison with existing elasto-plastic deformation models in the standard version of FRAPTRAN-1.5 [7]. In addition, a model for axial relocation of fuel pellet fragments within the distending cladding tube has been developed, implemented in FRAPTRAN-QT-1.5 and verified against LOCA simulation tests on high-burnup fuel rods [12, 15]. This relocation model is essential for estimating the amount of fuel pellet fragments that is free to move within the cladding tube. More specifically, it provides an upper bound for the amount of fuel that may be ejected through a cladding breach and dispersed into the coolant. The model accounts for the fuel fragment size distribution, but at present, it does not consider possible effects of axial gradients in rod internal gas pressure on fuel fragment axial relocation. A separate model for axial gas flow has recently been developed and implemented in FRAPTRAN-QT-1.5 [16], but it is not yet linked to the relocation model.

1.2 Scope and objective

As evidenced by the presentation in Section 1.1, most of the computational models needed for assessing fuel fragment dispersal from failed rods under LWR LOCAs are available in our extended version of FRAPTRAN-1.5, henceforth referred to as FRAPTRAN-QT-1.5. There is, however, a notable exception: the program lacks models by which the cladding rupture opening size can be estimated. Such a size estimate is needed for calculating the amount of fuel pellet fragments that may pass through the rupture opening, based on the calculated fragment size distribution and amount of axially mobile fragments. As of today, FRAPTRAN-QT-1.5 calculates the amount of dispersed fuel based on the assumption that

all fuel fragments above the cladding breach that are free to move downward by gravity will be ejected through the breach. This is a crude upper bound estimate, since the fuel dispersal will in many cases be limited by the dimensions of the cladding rupture opening.

The work presented in this report aims to formulate empirical models, by which the rupture opening dimensions in zirconium alloy cladding tubes that fail by ballooning and burst under typical LWR LOCA conditions can be estimated. The models are intended for implementation in FRAPTRAN-QT-1.5, hopefully leading to more realistic estimates of fuel pellet fragment dispersal in analyses of postulated LOCAs.

Section 2 of the report provides a review and analysis of available experimental data on cladding rupture opening dimensions, observed in LOCA simulation tests on single fuel rods as well as fuel assemblies (rod bundle tests). Tests performed on various zirconium-base cladding materials under typical LWR LOCA conditions with regard to environment conditions and thermal-mechanical loading are evaluated, with the aim to identify the most influential parameters for the rupture opening dimensions.

Section 3 starts with a review of a handful existing empirical models for the rupture opening dimensions. Following an assessment of these models against the experimental database in Section 2 of the report, a set of new empirical models is proposed that better reproduce the data.

Finally, Section 4 summarizes the work and the most important conclusions that can be drawn from it. Moreover, suggestions are also given for further model development.

2 Analysis of experimental data

Although a large number of studies have been conducted over the years on high-temperature ballooning and burst of zirconium alloy cladding tubes under LOCA conditions [8], there are only a few studies in which the cladding rupture opening dimensions have been systematically studied and properly reported: most studies have been concerned mainly with the ballooning behaviour and its potential to block coolant flow through the fuel assemblies. In the following, we assess the results of LOCA simulation tests on altogether 285 fuel rods, for which data on the cladding rupture opening dimensions have been reported in the open literature. All tests in the considered database were conducted on fuel rods with zirconium alloy cladding in steam environment, with sufficient steam supply to feed the high-temperature metal-water reactions without steam starvation.

Henceforth, the tests are divided into two categories: single rod tests and bundle tests. The advantage of single rod tests over bundle tests is first and foremost that the boundary conditions for the tested rod can be better controlled and monitored. On the other hand, bundle tests are probably more representative for the true accident conditions, since they reproduce rod-to-rod interaction and gradients in temperature and other properties across the fuel rod bundle. Hence, the two types of tests complement each other.

2.1 Single rod tests

All single rod LOCA simulation tests considered in this report were done in steam environment by heating a single internally overpressurized cladding tube sample at a time until the sample ruptured. The most important experimental parameters were the sample internal overpressure and heating rate. These parameters were usually not constant during a test, but varied during heat-up to an extent that depended on the test setup. The results from each test comprise time to cladding burst (rupture), burst temperature, hoop creep strain at burst, and dimensions of the rupture opening.

Eight different single rod test series, comprising totally 164 cladding samples, are considered in our assessment. Key parameters for these test series are summarized in Table 1. Except for the FR-2 and Halden series, the tests were done out-of-reactor. In most of these out-of-reactor tests, the cladding tubes were heated either by an internal electrical resistance heater or by an external infrared furnace. In the KfK-1988 test series, internal and external heating were combined. This, together with slow heating that allowed temperature gradients to be equilibrated by heat conduction, resulted in exceptionally uniform temperature distributions within the samples [17, 18]. In the BARC-2017 tests, direct electrical (Joule) heating was used. It seems that this kind of heating resulted in large temperature gradients in the samples, both in the axial and circumferential direction [19]. Moreover, the BARC-2017 tests were conducted on cladding tubes from Indian pressurized heavy water reactor (PHWR) fuel rods. The geometry of this cladding is different from that of typical LWR fuel cladding, which is the design studied in the other test series.

The FR-2 in-reactor tests were done on fresh (un-irradiated) and pre-irradiated test rodlets with Zircaloy-4 (Zr-1.4Sn-0.2Fe-0.1Cr by wt%) cladding, fuelled with UO_2 fuel pellets. In these tests, the cladding tube was heated by the nuclear fuel only (nuclear heating) [23, 24].

Table 1: Single rod burst tests conducted in steam, with data reported for cladding rupture opening dimensions. These data are presented in Section A.2, Appendix A.

Test series	# tests	Cladding material	Heating type	V_g [cm^3]	$\dot{T}$ [Ks^{-1}]	ΔP_b [MPa]	T_b [K]	ε_b [%]	σ_b [MPa]	w_b [mm]	l_b [mm]	A_b [mm^2]	Literature source
Out-of-reactor tests													
KfK-1988	25	Zr-4	Int+Ext	≈25	1	0.6 - 9.3	988 - 1285	24 - 106	5.7 - 96	-	-	1.4 - 287	[17, 18]
ANL-2008	8	Zr-2	External	≈10	5	6.4 - 9.1	1003 - 1063	36 - 61	47 - 67	0.8 - 5.1	10 - 17	-	[20]
ANL-2010	19	ZIRLO	External	≈10	5	4.0 - 8.8	946 - 1123	23 - 71	31 - 68	0.8 - 10	7.3 - 26	-	[21]
Stud-NRC	6	ZIRLO	External	10.4	5	8.1 - 10.9	953 - 1001	25 - 56	63 - 85	0.2 - 18	1.5 - 24	-	[4]
JAEA-2016	37	Zr-4	External	≈11	3 - 30	0.8 - 8.8	1042 - 1582	10 - 48	5.5 - 61	0.3 - 3.0	2.2 - 12	0.7 - 26	[22]
BARC-2017	25	Zr-4	Direct	≈14	5 - 19	0.6 - 7.3	871 - 1252	15 - 68	10 - 135	-	-	4 - 143	[19]
In-reactor tests													
FR-2	36	Zr-4	Internal	≈30	6 - 25	2.2 - 11.3	981 - 1288	26 - 67	15 - 78	0.1 - 11	4 - 62	-	[23, 24]
Halden	8	Zr-2/4,E110	Int+Ext	1.9 - 21.5	2 - 8	0.9 - 6.8	1028 - 1373	15 - 62	6.4 - 53	0.5 - 10	3 - 70	0.8 - 434	[3]
Total:	164	–	–	1.9 - 30	1 - 30	0.6 - 11.3	946 - 1582	10 - 106	5.5 - 135	0.1 - 18	1.5 - 70	0.7 - 434	

V_g: Sample internal gas volume; $\dot{T}$: Cladding heating rate during the test; $\Delta P_b, T_b$: Sample internal overpressure and cladding local temperature at burst; ε_b, σ_b: Cladding maximum hoop engineering strain and hoop nominal stress at time of burst; w_b, l_b, A_b: Circumferential width, axial length and area of the rupture opening.

The Halden IFA-650 series of in-reactor LOCA simulation tests were done on test rodlets with different designs that had been pre-irradiated to high or even very high fuel burnup [3]. In these tests, the cladding tube was heated both internally by the fuel pellets and externally by an electrical heater.

As evidenced by Table 1, the single rod tests considered in this report were done on different cladding materials. Also the cladding tube outer diameter and wall thickness differed significantly among the tests, and so did the axial length of the samples. The volume of pressurized gas available inside the cladding sample is important for the ballooning and burst behaviour. This volume, V_g, which includes the internal space of the sample itself as well as connected pressure lines, differed between the test series.

Table 1 summarizes the observed ranges for the cladding burst parameters ($\Delta P_b, T_b, \varepsilon_b, \sigma_b$) in each test series, and also the observed rupture opening dimensions. Here, w_b is the maximum width of the rupture opening in the circumferential direction of the cladding tube, l_b is the axial length, and A_b is the area of the rupture opening. It is usually unclear from the literature sources how these parameters were determined, but it seems that they were in most cases measured from front-view photographs of the rupture opening, as illustrated in Figure 1. Hence, A_b is most likely the orthographically projected area of the opening, determined either by use of image analysis software or some approximate method. The uncertainty in reported values for A_b is not stated in any of the literature sources. From Table 1, it is clear that a full set of dimensional parameters, i.e. w_b, l_b and A_b, is reported only for two of the eight studies considered here.

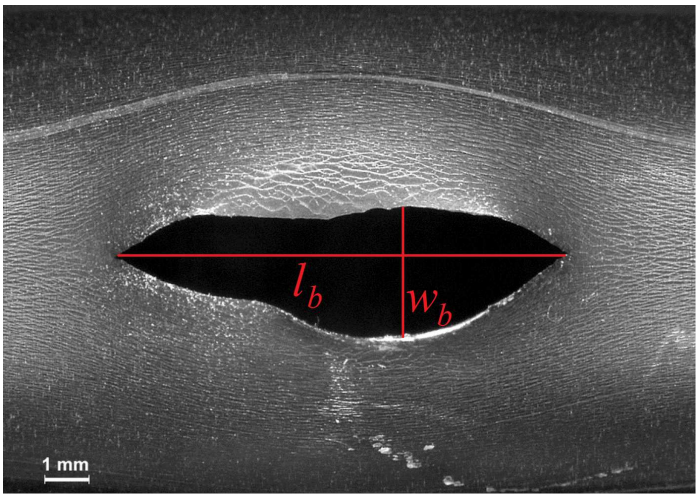

Figure 1: Definition of rupture opening dimensions w_b and l_b. Photograph from [25].

The majority of out-of-reactor tests listed in Table 1 were done on cladding material in as-fabricated state. However, the Studsvik-NRC series and part of the ANL-2008 series were done on irradiated cladding tubes, sampled from discharged LWR fuel rods. In addition, some tests in the ANL-2010 series were done on hydrogen-charged ZIRLO cladding. The test series summarized in Table 1 are further described in Section A.2 of Appendix A, where results from individual tests are also presented. It should be mentioned that data from five of the test series in Table 1 were used for calibration of models for cladding high-temperature creep and burst in a previous research project for SSM [9].

2.2 Bundle tests

The bundle tests considered in this report were conducted on bundles that comprised 21 electrically heated fuel rod simulators in the QUENCH facility at Karlsruhe Institute of Technology (KIT), Karlsruhe, Germany. Altogether seven bundle tests were performed under simulated PWR large-break LOCA conditions in the QUENCH-LOCA (QL) experimental series between 2010 and 2016. A summary of the experiments is given in [26].

Here, we consider six of the test series, as defined in Table 2. Five of the tests, QL1 - QL5, were done under nominally identical conditions: the only difference between these test is the cladding material. As-fabricated Zircaloy-4, M5 (Zr-1.0Nb-0.14O by wt%) and Optimized ZIRLO (Zr-0.7Sn-1.1Nb-0.11Fe-0.12O by wt%) claddings were used in QL1 - QL3, whereas QL4 and QL5 were done on M5 and Optimized ZIRLO that were charged with 100 and 300 weight parts per million (wppm) hydrogen, respectively, before testing. Since the nominal testing conditions were identical, these five tests allow a clear and straightforward comparison of the three different materials and assessment of possible effects of hydrogen on M5 and Optimized ZIRLO. However, all fuel rods in the QL1 - QL5 tests were pressurized to the same internal overpressure (5.2 MPa) before the simulated LOCA, which means that no information is available from these tests on how the rod internal pressure affects the rupture behaviour. Some information of this kind is available from the QL0 test, in which the test rods were pre-pressurized to internal overpressures in the range 3.2-5.2 MPa. The QL0 experiment was a commissioning test that was done on as-fabricated Zircaloy-4. The heating was slower than in the subsequent QL1 - QL5 tests.

Each bundle test in the QL-series resulted in data for 21 identical fuel rods that were brought to failure during the simulated LOCA. Each test therefore provides information on the typical spread in cladding burst properties. The data are particularly valuable for our assessment, since the full set of rupture opening parameters (w_b, l_b and A_b) is reported for each test rod in each bundle. The QL test series summarized in Table 2 are further described in Section A.3 of Appendix A, where results from individual fuel rods in the tested bundles are presented.

Table 2: Bundle tests conducted in the QUENCH-LOCA (QL) experiment series, with data reported for cladding rupture opening dimensions [26]. These data are summarized in Section A.3 of Appendix A. Each bundle comprised 21 identical, electrically heated fuel rod simulators with an internal gas volume (V_g) of 31.5 cm^3. Most of these rods failed by ballooning and burst during the tests. Average values for each bundle are given within brackets.

QL test	# burst rods	Cladding material	$\dot{T}$ [Ks^{-1}]	ΔP_b [MPa]	T_b [K]	ε_b [%]	σ_b [MPa]	w_b [mm]	l_b [mm]	A_b [mm^2]	Literature source
QL0	20	As-fabricated Zircaloy-4	2 - 3	3.2 - 5.1	1049 - 1141 (1095)	15 - 33 (21.4)	24 - 38	2.2 - 7.6 (3.9)	7.6 - 19 (12.7)	9.4 - 96 (33.0)	[25]
QL1	19	As-fabricated Zircaloy-4	7 - 8	≈5.2	1074 - 1163 (1128)	11 - 32 (20.2)	≈38	1.5 - 13 (4.2)	8 - 33 (15.3)	11 - 198 (47.0)	[27]
QL2	21	As-fabricated M5	7 - 8	≈5.2	1050 - 1195 (1138)	6 - 15 (11.2)	≈38	1.5 - 6.6 (3.1)	10 - 24 (13.3)	12 - 94 (29.0)	[28]
QL3	21	As-fabricated Opt ZIRLO	7 - 8	≈5.2	1064 - 1188 (1117)	9 - 18 (14.0)	≈38	2.6 - 6.2 (3.9)	11 - 20 (14.4)	17 - 67 (31.0)	[29]
QL4	19	M5 with 100 wppm H	7 - 8	≈5.2	1067 - 1151 (1107)	9 - 16 (11.8)	≈38	2.4 - 4.8 (3.3)	11 - 18 (13.1)	16 - 40 (24.1)	[30]
QL5	21	Opt ZIRLO with 300 wppm H	7 - 8	≈5.2	1027 - 1151 (1081)	10 - 22 (15.1)	≈38	2.7 - 4.9 (3.7)	12 - 18 (14.3)	19 - 52 (29.9)	[31]
Total:	121	–	2 - 8	3.2 - 5.2	1027 - 1195	6 - 33	24 - 38	1.5 - 13	7.6 - 33	9.4 - 198	

$\dot{T}$: Cladding heating rate during the test; $\Delta P_b, T_b$: Sample internal overpressure and cladding local temperature at burst; ε_b, σ_b: Cladding maximum hoop engineering strain and hoop nominal stress at time of burst; w_b, l_b, A_b: Circumferential width, axial length and area of the rupture opening.

2.3 Analysis of data

In the following subsections, the experimental database is analysed with regard to rupture opening shape and size, and how these properties are affected by cladding material conditions, such as alloy composition, hydrogen content and irradiation.

2.3.1 Rupture opening shape

Complete sets of dimensional parameters for the rupture opening, i.e. w_b, l_b and A_b, are reported from the JAEA-2016 and the QUENCH-LOCA experimental series; see Tables 1 and 2. These data make it possible to find an empirical relation between the area, A_b, and the linear dimensions, w_b and l_b, of a typical rupture opening. To this end, we write

$$A_b = C_A w_b l_b, \tag{1}$$

with the aim to find a best-estimate value for the constant C_A by use of the aforementioned experimental series. We note that, for a rupture opening with rhombic shape, $C_A = 1/2$. Likewise, an elliptic rupture opening has $C_A = \pi/4$. These values for C_A are compared with experimental data for A_b versus the product $w_b \times l_b$ in Figure 2. Obviously, the data generally fall between the lines representing rhombic and elliptic rupture openings. More precisely, a best fit to the JAEA-2016 data yields $C_A = 0.708$, whereas a best fit to the QL0-QL5 data yields $C_A = 0.592$. The difference between the two data sets suggests that large rupture openings have a near rhombic shape, while small openings tend to be more elliptic; see Figure 2. However, there may be other factors than rupture opening size that cause the difference between these two data sets. A best fit to both sources of data gives $C_A = 0.619$. This value for C_A will henceforth be used for estimating A_b from measured w_b and l_b or vice versa. Hence, possible differences in C_A between small and large rupture openings will be neglected.

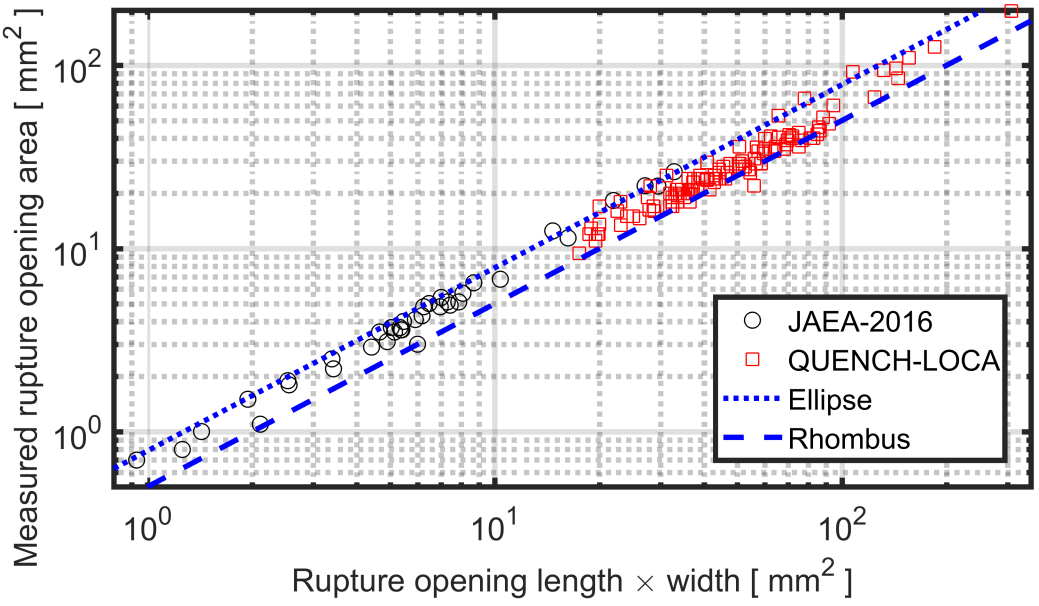

Figure 2: Measured area, A_b, versus product of measured linear dimensions for the rupture opening. The lines correspond to elliptic and rhombic rupture openings, respectively.

Next, we assess the length-to-width ratio of the rupture opening. Figure 3 is a compilation of data for l_b/w_b from five experiment series. Notwithstanding significant scatter, especially for small rupture openings, there is a clear trend in the data: the shape changes from crack-like ($l_b/w_b > 10$) for small rupture openings to mouth-like ($l_b/w_b \approx 2$) for large openings. We note that the rupture opening width w_b is usually less than the cladding outer diameter, D_o.

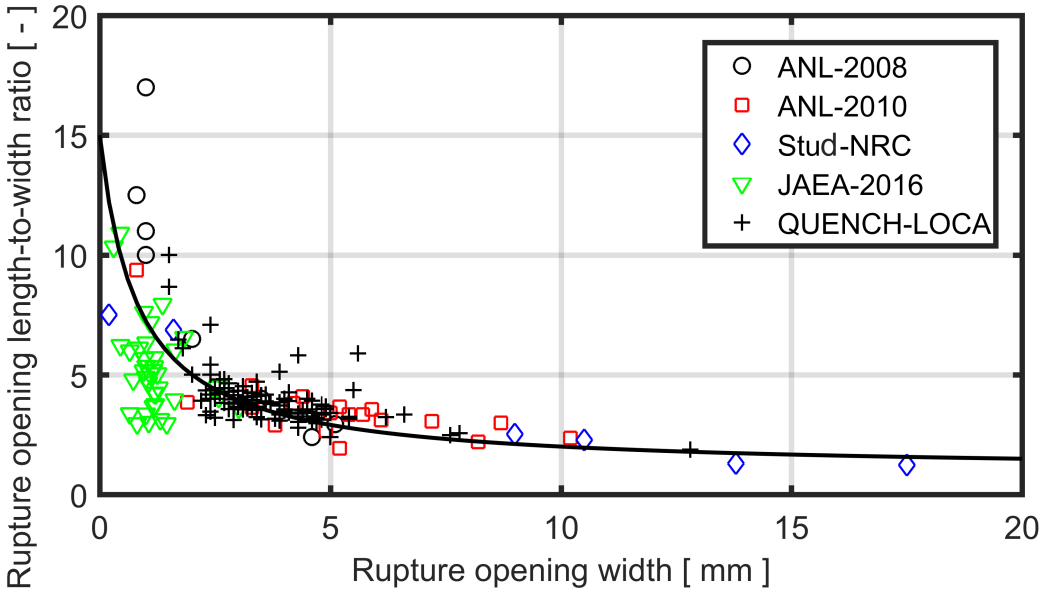

Figure 3: Measured length-to-width ratio (l_b/w_b) versus rupture opening width, w_b.

The solid line in Figure 3 is an empirical fit to the data, given by the relation

$$\frac{l_b}{w_b} = \frac{11.4}{w_b + 0.81} + 0.95, \tag{2}$$

where the expected unit for w_b is mm. By combining equations (1) and (2), it is possible to estimate A_b, w_b or l_b from any of the other two parameters. For example, A_b can be calculated from w_b through (w_b in mm):

$$A_b = 0.619 w_b^2 \left(\frac{11.4}{w_b + 0.81} + 0.95 \right). \tag{3}$$

This is a useful, however approximate, relationship for estimating missing dimensional parameters in reported rupture opening data. For illustration, w_b was estimated from measured values of A_b in the JAEA-2016 and QUENCH-LOCA test series by inverting equation (3). The estimated values for w_b are compared with their true measured values in Figure 4. The estimated values are in fair agreement with the true values, except for the range $4 < w_b < 6$ mm.

An important conclusion that can be drawn from Figure 3 is that the rupture opening width, w_b, is the most important dimensional parameter with regard to possible dispersal of fuel pellet fragments. The width, rather than the length or area, of the rupture opening will be the limiting dimensional parameter that determines whether fuel pellet fragments of a given size may be ejected through the cladding breach. The typical fuel fragment size depends on the operational history of the fuel and can be estimated through empirical relations [12].

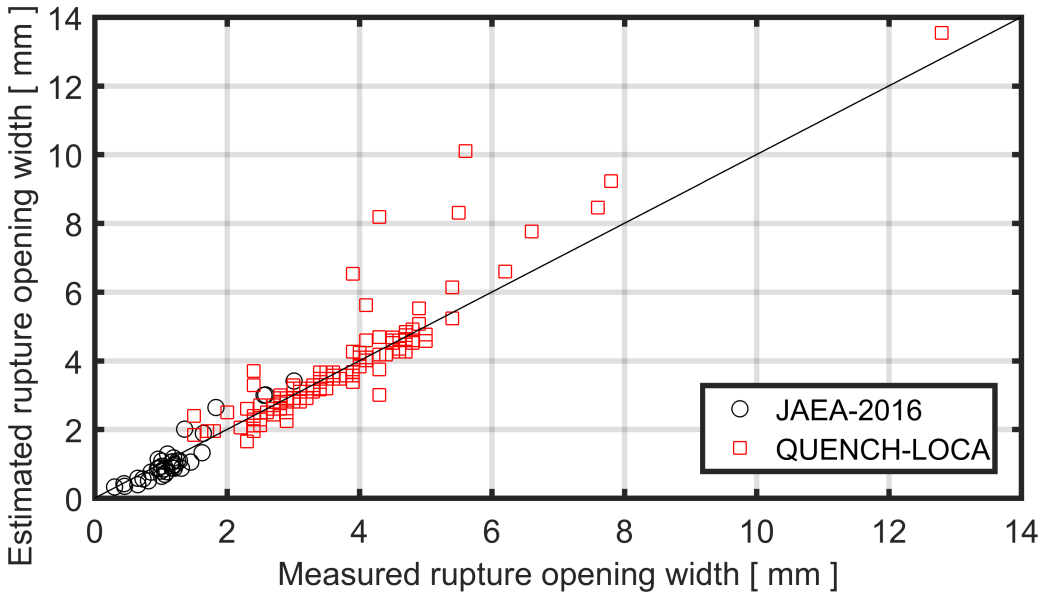

Figure 4: Rupture opening width, w_b, estimated from measured rupture opening area A_b through the inverse of equation (3), in comparison with true measured data for w_b.

2.3.2 Rupture opening size

Available cladding burst test data from experiments conducted under simulated LWR LOCA conditions show that the rupture opening area correlates with the sample overpressure and temperature at time of burst. This is illustrated by Figures 5 and 6, which in addition to available data also include empirical upper-bound limits proposed in literature; see Section 3.1. It is important to remember that burst temperature and burst overpressure cannot be considered as independent parameters in the LOCA simulation experiments considered here. As explained in Section 2.1, the samples were pressurized to various internal overpressures and then heated until the cladding ballooned and ruptured. Figure 7 shows the relation between sample overpressure and temperature at time of burst for the entire database of 285 samples. The parameters are clearly dependent.

In fact, burst overpressure is not a good parameter, unless all samples have identical diameter and wall thickness. The nominal hoop burst stress, as calculated through equation (A.2), is a better parameter if there are differences in cladding tube dimensions among the samples. This is illustrated by Figure 8: the correlation between burst stress and burst temperature is clearer than that between burst overpressure and burst temperature, since the influence of cladding tube dimensions is accounted for by the stress.

The data for rupture opening area are plotted versus nominal hoop burst stress in Figure 9. Obviously, there is a fairly sharp threshold at 30-40 MPa: below this stress, only small rupture openings are observed. Above the threshold, the rupture opening areas vary over a wide range, also within test series where testing conditions are nominally identical for all samples. A good example is the QL1 bundle test, which was conducted on electrically heated fuel rod simulators with as-fabricated Zircaloy-4 cladding; see Section A.3.2 in Appendix A. The nominal hoop burst stress was 38 MPa in all rods within the bundle, which is just at the aforementioned stress threshold. The measured rupture opening area varied by a factor of 18 among the 19 failed rods in the bundle, from 11 to 198 mm^2. This

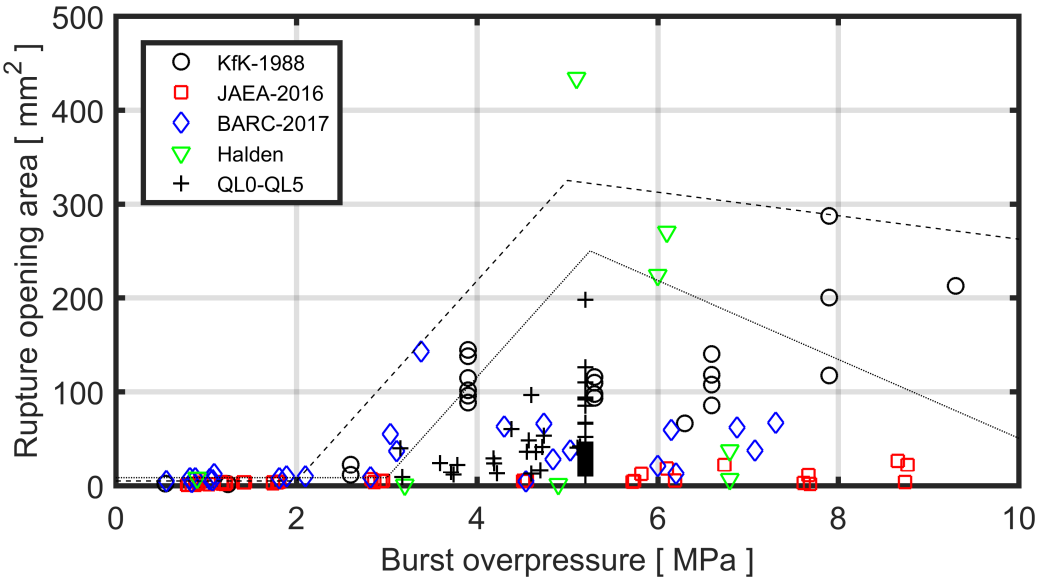

Figure 5: Measured rupture opening area, A_b, versus sample overpressure at time of burst, ΔP_b. Dashed and dotted lines are empirical upper-bound limits for irradiated and un-irradiated cladding, proposed in [5]; see Section 3.1.

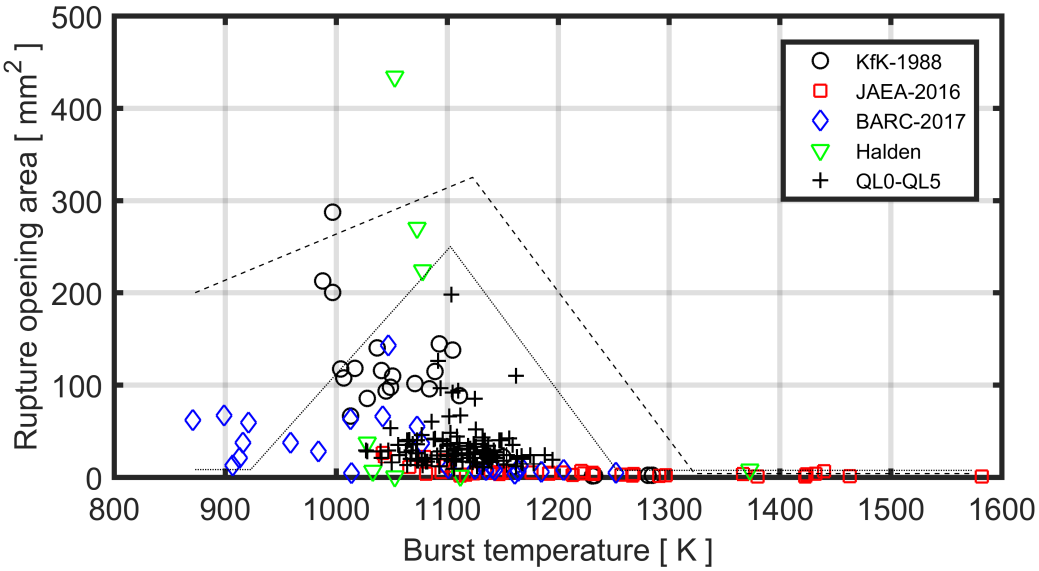

Figure 6: Measured rupture opening area, A_b, versus sample temperature at time of burst, T_b. Dashed and dotted lines are empirical upper-bound limits for irradiated and un-irradiated cladding, proposed in [5]; see Section 3.1.

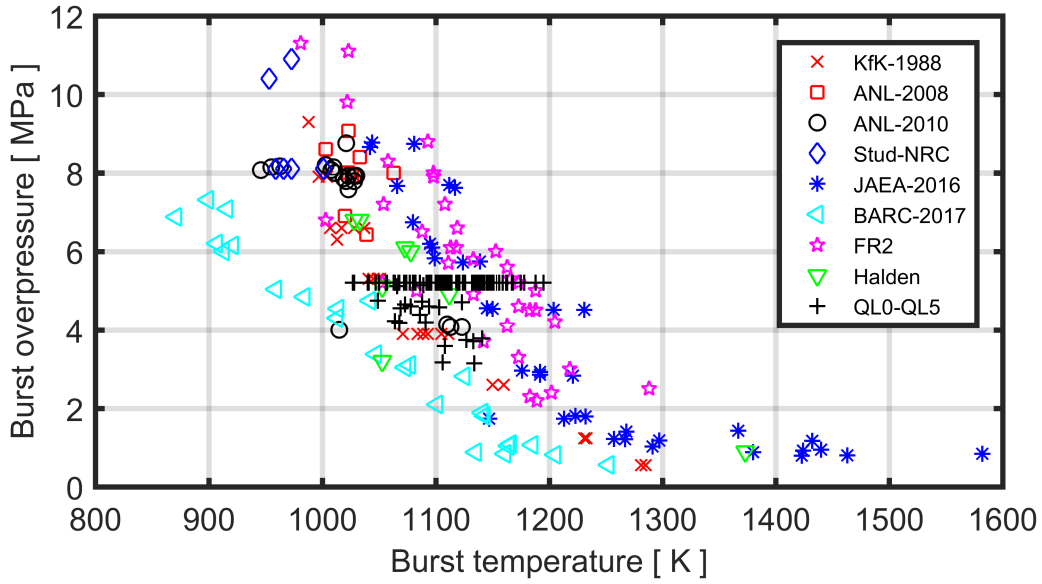

Figure 7: Burst overpressure versus burst temperature for the 285 samples in the considered database.

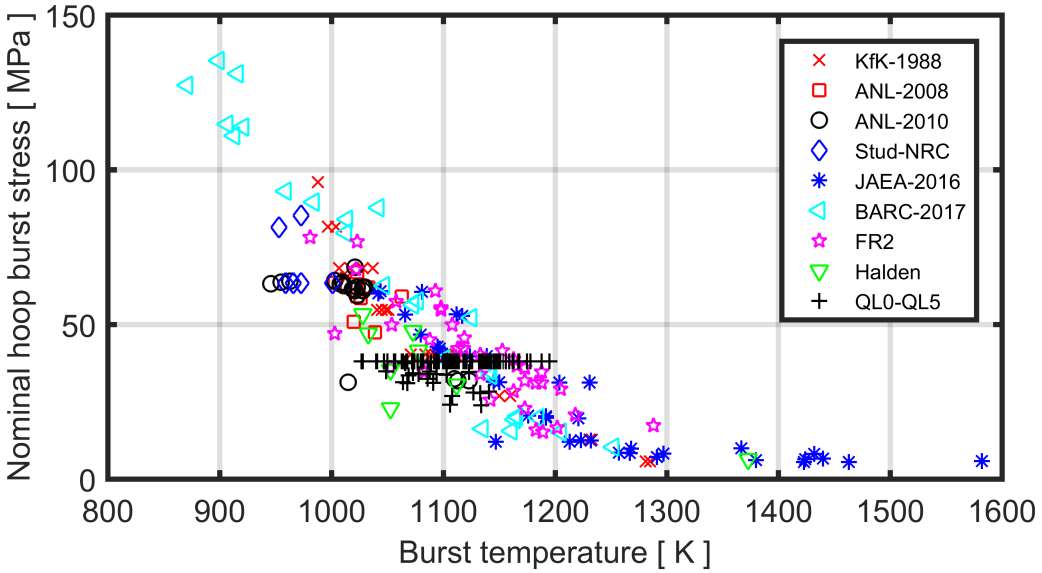

Figure 8: Nominal hoop burst stress versus burst temperature for the 285 samples in the considered database.

is a very large spread: the standard deviation for A_b is 49 mm^2 and the mean value is 47 mm^2. For comparison, the cladding burst temperature varied merely from 1074 to 1163 K among the failed rods in the QL1 test; see Table A.11.

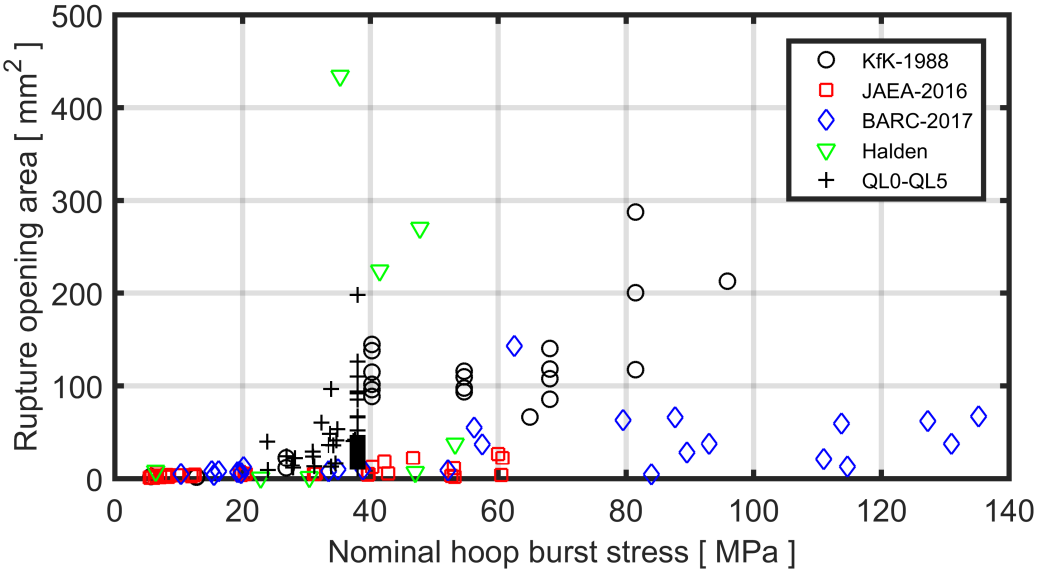

Figure 9: Measured rupture opening area, A_b, versus cladding nominal hoop stress at time of burst, σ_b.

2.3.3 Causes to the spread in rupture opening data

Except for cladding samples that failed at low internal overpressure and hoop stress, there is a large spread in the rupture opening data considered in this report. As mentioned above, the spread is not only between test series, but also within test series where testing conditions are nominally identical for all samples. The fundamental reason for this variability is that cladding high-temperature ballooning and burst are caused by plastic instability, a phenomenon where small local perturbations in material properties and/or thermal-mechanical loading conditions have a large impact on the deformation and subsequent failure of the cladding tube. Early theoretical studies, using perturbation analyses of a pressure-loaded, nominally axisymmetric cladding tube under time-dependent and/or time-independent plastic deformation, showed that the deformation is extremely sensitive to deviations from axial symmetry [32]. The latter can be geometrical imperfections of the tube or circumferential temperature gradients, caused by non-symmetric cooling or eccentrically positioned fuel pellets within the tube. More precisely, the analyses showed that also very moderate deviations from axial symmetry lead to localization of the deformation along the circumference, bending of the tube and to cladding rupture at a lower overall hoop strain than if the configuration had been perfectly axisymmetric.

Later studies have confirmed the importance of circumferential temperature differences experimentally [17, 33] and models have been developed to account for the phenomenon [34–36]. Also the effects of geometrical imperfections on ballooning and burst have been further studied [37, 38]. The analysis in [38] showed that even very shallow surface defects, e.g. arising from a non-uniform or partially spalled oxide layer, significantly reduce

the overall hoop strain to cladding failure by localizing the plastic deformation to the defect.

In conclusion, theoretical and computational analyses, as well as experiments, show that even small deviations from axial symmetry reduce the overall hoop strain to cladding failure in burst tests. It is therefore reasonable to believe that much of the scatter in cladding burst strain data from LOCA simulation tests is caused by random deviations from axial symmetry, not least with regard to the cladding temperature distribution. As mentioned in Section 2.1, cladding burst tests done with combined internal and external heating, such as in the KfK-1988 and Halden IFA-650 series, result in nearly uniform cladding temperature distributions and large burst strains. Likewise, slow heating usually results in a more uniform temperature distribution than fast heating, since heat conduction within the cladding has time to equilibrate circumferential and axial temperature gradients. The question is whether the observed variability in rupture opening data can be attributed to random deviations from axial symmetry in the tests, just like the burst strain data? We note from Figure A.2 in Section A.2.1 of Appendix A that the spread in A_b reported from the KfK-1988 test series is moderate, which speaks in favour of this hypothesis: as already mentioned, the cladding temperature was well controlled and nearly uniform[1] in these tests. On the other extreme are the QUENCH-LOCA bundle tests, where the cladding temperature difference between the hot and cold side of individual rods in the bundle reached up to 100 K or even higher: the amplitude of the circumferential temperature difference depended on the position of the rod within the bundle [26]. This rod-to-rod variation may very well explain the large variability in rupture opening data reported for each of the QUENCH-LOCA experiments; see Section A.3 in Appendix A.

However, to the author's best knowledge, there are currently no experimental studies that give clear evidence for a reduction in rupture opening size as a result of circumferential temperature gradients or other deviations from axial symmetry. Nevertheless, Narukawa and Amaya [39] have addressed the subject by comparing their burst test results (JAEA-2016 test series, see Section A.2.5 in Appendix A) with those reported from the KfK-1988 series. Based on this comparison, they stated that both the burst strain and the rupture opening dimensions are reduced by circumferential temperature gradients. If their statement is correct, the rupture opening size should correlate with the hoop burst strain. From Figures 10 and 11, it is impossible to see such a correlation when the entire database is considered. However, it can be seen for the JAEA-2016 and KfK-1988 test series.

Narukawa and Amaya pointed out that not only circumferential but also axial temperature gradients may localize the cladding deformation and reduce the rupture opening [39]. While the axial temperature distribution may vary significantly from one test facility to another, due to differences in heated length, the sample-to-sample variation within a specific facility is usually moderate, at least for single rod burst tests. With regard to the spread in rupture opening data, it is therefore reasonable to believe that random variations in the temperature distribution along the samples are less important than random variations in the circumferential direction.

For irradiated cladding samples, additional localization effects linked to non-uniform corrosion or loss of axial symmetry by e.g. ovalization of the cladding during long-term reactor

[1] According to [17], temperature differences along the cladding circumference were < 10 K in the KfK-1988 test series.

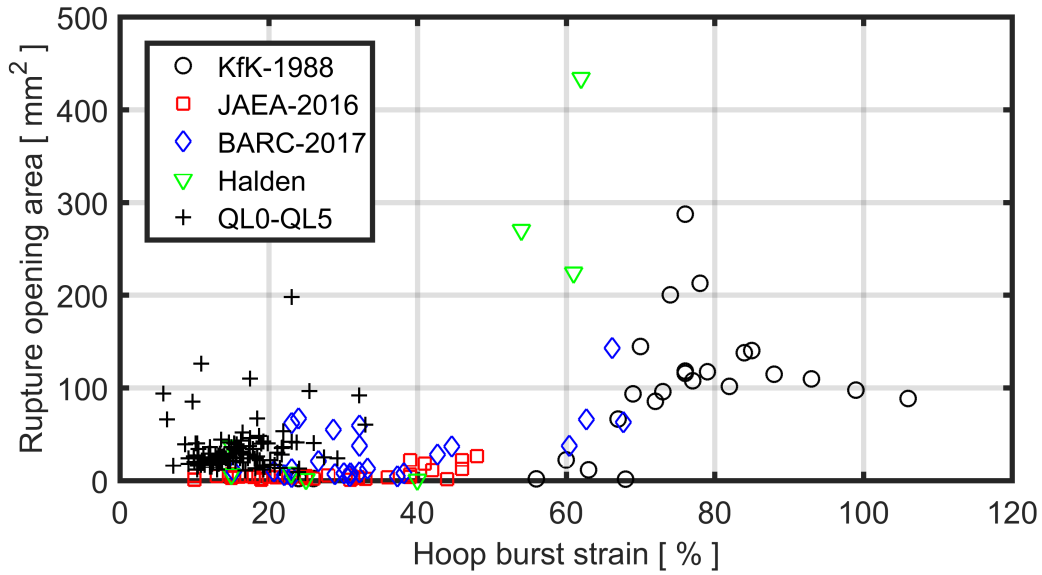

Figure 10: Measured rupture opening area, A_b, versus cladding hoop burst strain, ε_b.

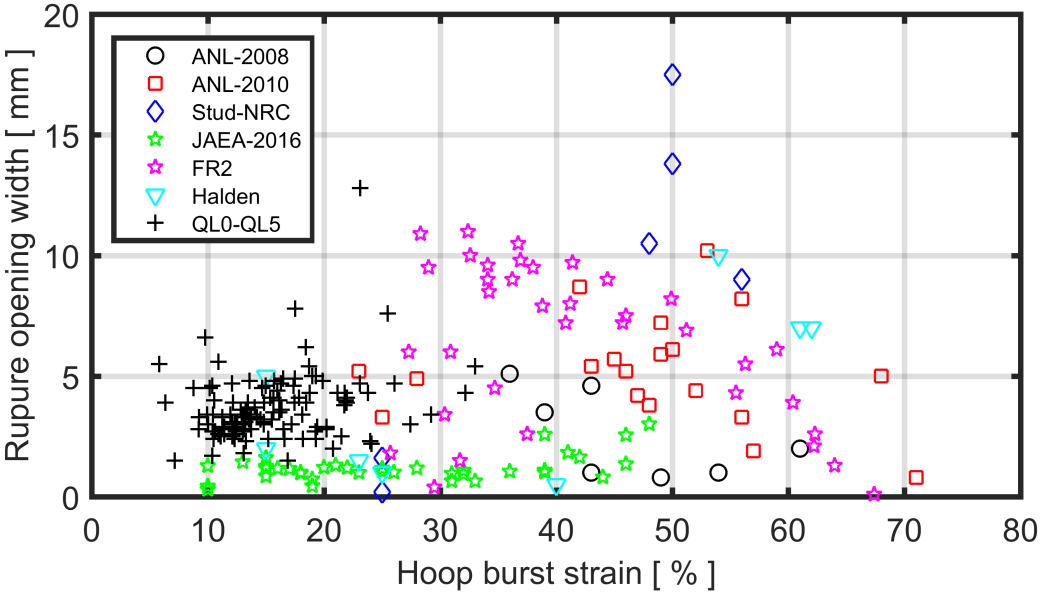

Figure 11: Measured rupture opening width, w_b, versus cladding hoop burst strain, ε_b.

operation may add to the localization of high-temperature deformation. Hence, we may expect that the variability in burst strain and rupture opening data is larger for pre-irradiated than for as-fabricated cladding. We may also expect that burst openings tend to be smaller for pre-irradiated samples with significant corrosion. This hypothesis is supported by the Halden IFA-650.5 test rod (75 μm thick oxide), which had a remarkably small rupture opening. However, the pre-irradiated samples in the ANL-2008 test series, which had only 10 μm thick oxide, do not show any reduction in rupture opening compared with as-fabricated samples; see Figures A.3 and A.4.

2.3.4 Differences between cladding materials

The QUENCH-LOCA bundle tests QL1, QL2 and QL3 were done on electrically heated fuel rod simulators that were clad with as-fabricated Zircaloy-4, M5 and Optimized ZIRLO material; see Section A.3.2. Since the cladding material was the only difference among these tests, it is possible to identify differences between the materials with regard to burst behaviour.

Although there is a large spread in data from each bundle test, significant differences are found for the *average* values of ε_b and A_b reported from QL1, QL2 and QL3; see Table 2. Obviously, Zircaloy-4 has the largest average values for ε_b and A_b , whereas M5 has the smallest. The same ordering of the materials holds for w_b and l_b, but the differences between the average values of these two parameters are smaller.

The aforementioned differences pertain to cladding materials in as-fabricated condition. Whether they persist during in-reactor operation of the fuel is unclear, since there are very few burst tests conducted on pre-irradiated cladding materials other than Zircaloy-4.

2.3.5 Effects of irradiation

The largest source of data for identifying possible effects of irradiation and long-term in-reactor operation on the cladding burst behaviour is the FR2 series of in-reactor tests; see Section A.2.7. Based on the results of these tests, the investigators concluded that there was no influence of pre-irradiation (characterized by fuel pellet burnup in the range from 0 to 36.5 MWd(kgU)$^{-1}$) on the cladding burst behaviour [24]. This conclusion is consistent with the data for w_b presented in Figures A.13 and A.14. However, the pre-irradiation conditions in the FR2 were not typical for light water reactors: due to the low (330 K at inlet) coolant water temperature in the FR2 core, the cladding corrosion was negligible, even for test rods that had been pre-irradiated to 36.5 MWd(kgU)$^{-1}$ in the reactor [24].

Effects of pre-irradiation on the rupture opening width w_b are evident in the results from the ANL-2008 test series on Zircaloy-2 cladding. More precisely, the pre-irradiated samples have wider openings than un-irradiated samples; see Figures A.3 and A.4. Strangely enough, an opposite trend can be seen for the hoop burst strain. Unfortunately, there are only three pre-irradiated samples in this test series, for which rupture opening dimensions have been reported in the open literature. It is therefore difficult to draw any definite conclusions from the aforementioned observations.

Finally, it is worthwhile to compare results for as-fabricated versus pre-irradiated ZIRLO

cladding of the first generation, reported from the ANL-2010 and Studsvik-NRC test series. The testing conditions were similar in these two series; see Sections A.2.3 and A.2.4 in Appendix A. A comparison of the rupture opening widths reported for pre-irradiated samples in the Studsvik-NRC study versus un-irradiated as-fabricated (AF) and hydrogen-charged (HC) samples in the ANL-2010 study is shown in Figure 12. The spread in data is large for the pre-irradiated samples, which makes it impossible to draw any definite conclusion regarding possible effects of irradiation on w_b: the very wide burst openings observed for two of the Studsvik-NRC samples may be an effect of the exceptionally high burst stress.

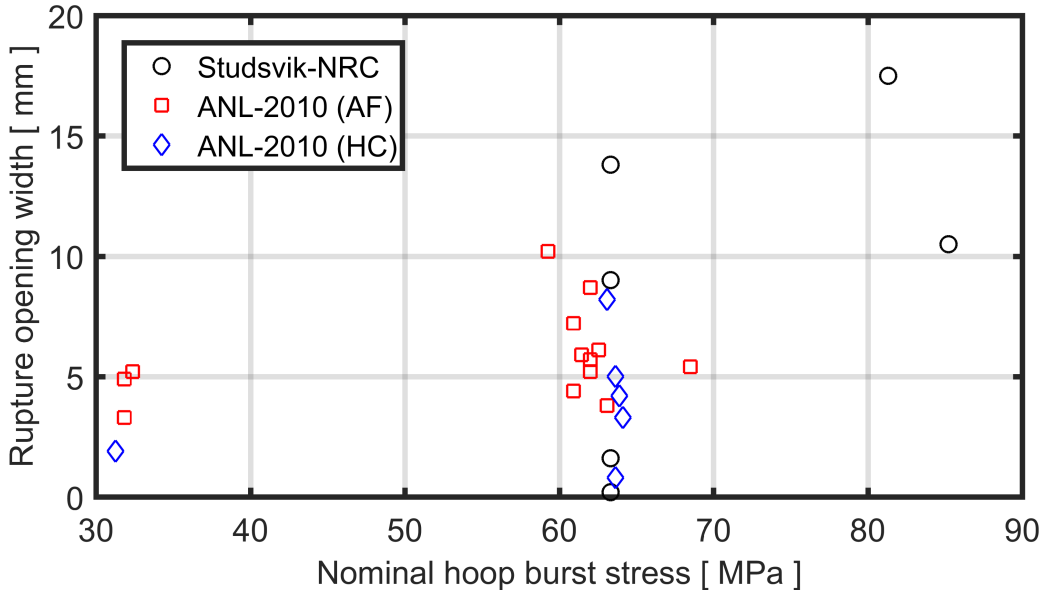

Figure 12: Measured rupture opening width, w_b, reported from single rod burst tests on first generation ZIRLO cladding in pre-irradiated (Studsvik-NRC) versus un-irradiated condition (ANL-2010). The un-irradiated samples are either in as-fabricated (AF) or hydrogen-charged (HC) state; see Section A.2.3.

In conclusion, the considered database on cladding rupture opening dimensions provides no clear evidence of pre-irradiation effects. However, if such effects do exist, the ANL-2008 and Studsvik-NRC test series suggest that the rupture opening would be wider for pre-irradiated than for un-irradiated (fresh) cladding materials: there are no indications, whatsoever, of an opposite trend.

2.3.6 Effects of hydrogen

The effects of hydrogen on the burst behaviour of un-irradiated cladding materials can be assessed by comparing results from burst test series conducted on samples that have been charged with hydrogen to various concentrations. Let us first consider the QUENCH-LOCA bundle tests, where M5 cladding in as-fabricated state (test QL2) can be compared with material charged with 100 wppm hydrogen (test QL4). Likewise, Optimized ZIRLO cladding in as-fabricated state (test QL3) can be compared with material charged with 300 wppm hydrogen (test QL5). The rupture opening widths measured in these two pairs of experiments are shown in Figures A.21 and A.22 in Section A.3.2. As can be seen from these figures and from the average values for the burst parameters in Table 2, the results are very similar for the two materials: The hydrogen has no effect on the rupture opening

dimensions w_b, l_b and A_b, but the burst temperature is 30-40 K lower for the hydrogen-charged materials.

A similar reduction in burst temperature can be seen for hydrogen-charged samples in the ANL-2010 test series on un-irradiated ZIRLO cladding of the first generation; see Figures A.5 and A.6 in Section A.2.3. The hydrogen concentration in the six hydrogen-charged samples ranged from 220 to 700 wppm, which means that the burst behaviour of the samples is more or less affected by hydrogen [21]. In addition to the reduction in burst temperature, the results suggest that there is also a slight reduction in rupture opening width for the hydrogen-charged samples. However, a firm conclusion on this issue cannot be drawn on the basis of only six tested samples. In fact, a recent experimental study on ballooning and burst of hydrogen-charged samples of Zircaloy-4 cladding in inert (argon) atmosphere rather than steam showed that the rupture opening was larger in hydrogen-charged samples than in as-fabricated samples [40].

The decrease in cladding burst temperature for hydrogen charged samples observed in the QUENCH-LOCA and ANL-2010 test series is consistent with the effect of hydrogen on the α $(\alpha+\beta)$ phase transition temperature, T_α, for zirconium alloys. This effect is illustrated for Zircaloy-4 in Figure 13, which shows that T_α decreases with increasing concentration of hydrogen in the cladding metal. The reader is referred to [41, 42] and references therein for further information on hydrogen effects on the phase composition of zirconium alloys.

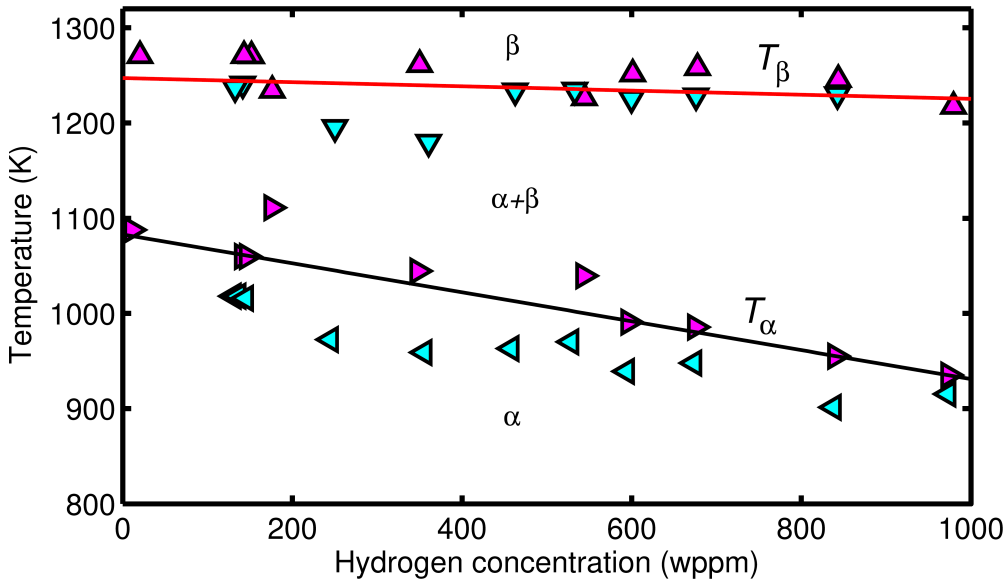

Figure 13: Calculated phase boundary temperatures (solid lines) versus cladding metal layer excess hydrogen concentration, in comparison with data for low-tin Zircaloy-4. The lines discriminate data for heating (△▷) and cooling (▽◁), presented by Brachet and co-workers [43], and are assumed to represent the equilibrium phase boundary temperatures [41, 42].

3 Empirical models

3.1 Existing models

Empirical models, intended to correlate cladding rupture opening dimensions to key parameters, such as cladding temperature or overpressure at time of burst, have been proposed as supplement to the results of various burst test series. An early example is the work by Chung and Kassner [44], who formulated upper-bound correlations for the rupture opening area A_b versus burst temperature and sample overpressure, based on their own burst test results for as-fabricated Zircaloy-4 cladding. It should be remarked that they conducted the tests with very limited steam supply, which obviously led to steam starvation that affected the burst behaviour at high temperature. This is the reason for not considering their burst test results in this report. A similar upper-bound correlation for A_b versus T_b was presented by Markiewicz and Erbacher, based on their KfK-1988 burst test results on Zircaloy-4 [17]. Figure 14 shows these two upper-bound models, together with their supporting data. The limits differ at low and high temperature, but they both exhibit a substantial reduction in A_b when the temperature increases from about 1100 to 1180 K, i.e. just above the $\alpha \quad (\alpha+\beta)$ phase transition temperature; compare Figure 13.

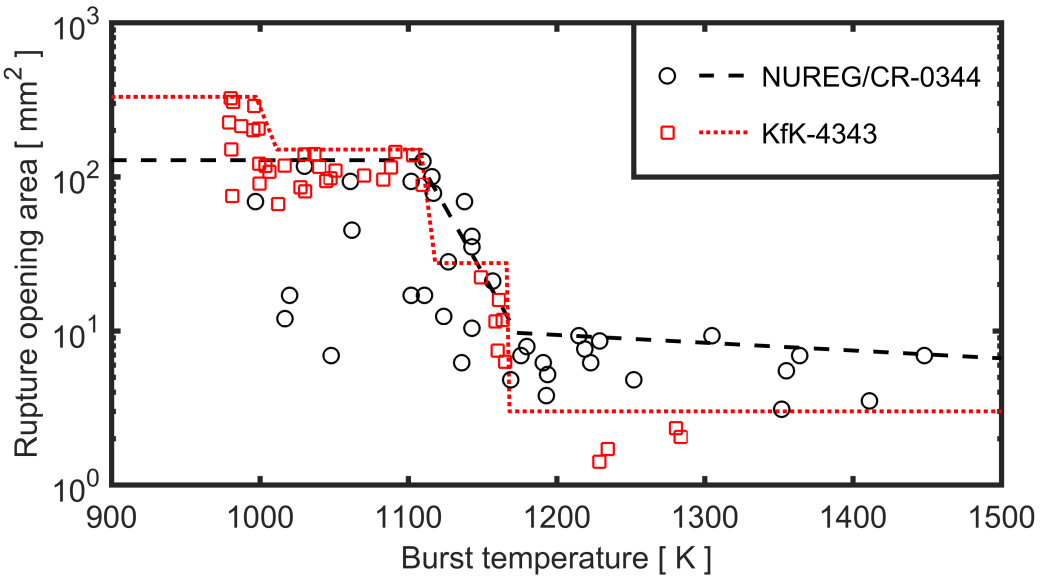

Figure 14: Empirical upper-bound limits for the rupture opening area A_b versus burst temperature T_b, proposed for Zircaloy-4 cladding by Chung and Kassner (NUREG/CR-0344) [44] and Markiewicz and Erbacher (KfK-4343) [17].

A more recent example is by Narukawa and Amaya [39], who proposed a best-estimate correlation for A_b versus the product $\sigma_b \times \varepsilon_b$. This unconventional choice of abscissa fitted their own (JAEA-2016) Zircaloy-4 burst test results fairly well, but the correlation between $\sigma_b \times \varepsilon_b$ and A_b for other burst test series is weak.

Hence, most existing models for the cladding rupture opening dimensions are empirically formulated on the basis of individual burst test series. Their capability to reproduce a larger set of data, comprising several burst test series, is generally poor. To the author's best knowledge, the only empirical model that has been fitted to a wider set of burst test

data is presented in the aforementioned NEA/CSNI report on fuel fragmentation, relocation and dispersal [5]. This model provides upper-bound limits for A_b versus burst temperature and burst overpressure[2] for un-irradiated and irradiated cladding separately. The limits are shown in Figures 5 and 6, together with burst test data from the experimental studies compiled in Appendix A. Since this database is more extensive than that used for formulating the NEA/CSNI empirical limits, the latter do not completely bound the database as intended with upper-bound models.

3.2 Proposed models

The work in this report is aimed to formulate empirical models for the cladding rupture opening dimensions, based on the burst test data compiled in Appendix A and analysed in Section 2.3. From the assessment of reported data for the rupture opening shape in Section 2.3.1, we concluded that the circumferential width, w_b, is the most important dimensional parameter of the rupture opening with regard to possible dispersal of fuel pellet fragments. The width, rather than the length or area, of the rupture opening will be the limiting dimensional parameter that determines whether fuel pellet fragments of a given size may be ejected through the cladding breach. Consequently, we seek a correlation for w_b with regard to suitable parameters. More precisely, the parameters entering the correlation should be strongly influential for w_b, they should be available from the experimental studies, and finally, they should be easy to calculate with computer programs used for fuel rod thermal-mechanical analyses, such as FRAPTRAN. With these requirements in mind, the following parameters can be identified as suitable candidates in empirical correlations for w_b, based on our assessment of the database:

- Burst temperature, T_b;
- Burst overpressure, ΔP_b, or cladding nominal hoop stress at time of burst, σ_b. As already noticed in Section 2.3.2, the nominal hoop burst stress is clearly a better parameter than the burst overpressure, since it accounts for differences in cladding tube dimensions;
- Product of the burst overpressure and the free gas volume inside the cladding tube, $\Delta P_b \times V_g$. This product is a measure of the total stored energy in the enclosed and overpressurized gas. Part of this energy will drive the cladding deformation upon rupture.

From Figures 7 and 8, it is clear that T_b correlates with both ΔP_b and σ_b. Hence, it is not meaningful to include more than one of these parameters in a correlation for w_b.

We note that hoop burst strain, ε_b, is unsuited as a parameter, for two reasons: it does not correlate with w_b (see Figure 11), and it is difficult to calculate (predict) with fuel rod analysis computer programs [9]. Likewise, the product $\Delta P_b \times V_g$ may be difficult to calculate for high-burnup fuel rods. The reason is that axial gas communication is restricted inside high-burnup fuel rods, and consequently, that only part of the free gas volume may be instantly available for driving the cladding ballooning and burst. In fact, also for cladding

[2]The empirical limits in [5] are actually defined with sample burst pressure (P_b) rather than burst overpressure (ΔP_b) as abscissa. Since the system pressure in the considered test facilities is up to 0.3 MPa, this is the maximum difference between P_b and ΔP_b in the database supporting the limits.

samples with excellent internal gas communication, the correlation between w_b and $\Delta P_b \times V_g$ is usually no better than that between w_b and ΔP_b alone. The reason is probably that only part of the elastic energy in the overpressurized gas contributes to the formation of the cladding breach, and that this energy is more or less independent of the totally stored energy $\Delta P_b \times V_g$.

Other parameters that may influence w_b were assessed in Sections 2.3.4-2.3.6. These parameters include cladding type (Zircaloy-4, M5, ZIRLO), irradiation and cladding hydrogen concentration. We concluded that hydrogen concentration has no noticeable effect on w_b, and that the effect of irradiation is unclear, due to the scarcity of data from burst tests on irradiated cladding samples. However, existing data show no dramatic effect of irradiation on w_b. Cladding type was found to have a noticeable effect: w_b was on average 26 % lower for M5 cladding than for Zircaloy-4 under nominally identical testing conditions. Data for w_b from burst tests on Optimized ZIRLO cladding fall between these two alloys; see Table 2. These differences are observed for as-fabricated cladding materials, and it is not clear whether they persist during in-reactor operation: as of today, there are very few burst tests conducted on irradiated cladding materials other than Zircaloy-4.

In addition, it is likely that w_b is affected by deviations from axial symmetry, such as circumferential temperature differences in the cladding. However, these effects are rarely quantified in experiments, and most computational analyses of the fuel rod behaviour are done under the assumption of axial symmetry. Hence, possible effects of circumferential temperature differences or other deviations from axial symmetry on w_b must be neglected.

Based on the assessment of available data on cladding rupture opening dimensions from LOCA simulation tests, the following empirical correlation is proposed for the circumferential width of the rupture opening, w_b:

$$w_b(\sigma_b) = \alpha D_o \left(1 - e^{-\beta(\sigma_b - \sigma_{th})}\right). \tag{4}$$

Here, D_o is the as-fabricated outer diameter of the cladding tube, and σ_b is the nominal hoop stress at burst, which is calculated from the burst overpressure and cladding as-fabricated dimensions through equation (A.2). The remaining parameters in equation (4) are constants that were fitted to the burst test database in Appendix A. More precisely, σ_{th}=5.0 MPa was fitted directly by inspection of the data. This is a threshold hoop stress that must be transgressed for the cladding breach to open. Once σ_{th} was settled, the parameters α and β were determined such that the l^2-norm (Euclidian norm) of absolute differences between calculated and measured values for w_b was minimized. A Nelder-Mead [45] optimization algorithm, available in the MATLAB Optimization Toolbox [46], was applied for this purpose. The database used for determining the best-estimate values for α and β consisted of two types of data: i) 235 burst tests, for which w_b was directly measured and reported; ii) 50 burst tests, for which w_b was estimated from measured and reported values for A_b by inverting equation (3). The latter type of data comprise the KfK-1988 and BARC-2017 burst test series.

A fit to the entire database of 285 burst tests gives the best-estimate values α=0.5848 and β=3.35$\times 10^{-8}$ Pa^{-1}. Figure 15 shows the results of equation (4) with these best-estimate values for α and β, in comparison with the supporting database. The calculations were done with D_o=9.13 and 15.20 mm, corresponding to the min/max cladding diameters represented in the database.

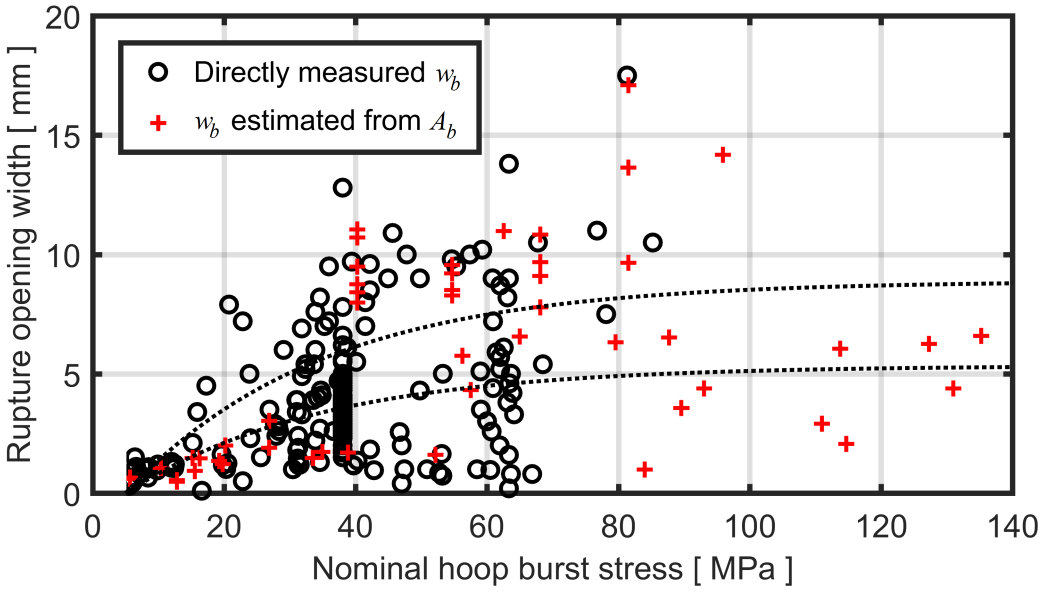

Figure 15: Range of best-estimate ($\alpha = 0.5848$) rupture opening widths in comparison with the supporting database. Dotted lines correspond to equation (4) with cladding outer diameter D_o=9.13 and 15.20 mm, which is the range spanned by the database.

Since the cladding outer diameter $D_o$differs between the considered test series, it may be more appropriate to compare calculated versus measured rupture opening widths for each test series separately. Such a comparison is shown in Figure 16. Obviously, the predictability of the model is rather poor.[3] In particular, calculated values for w_b approach αD_o for tests performed with a burst stress exceeding about 40-50 MPa, while measured values for w_b are very scattered in such tests.

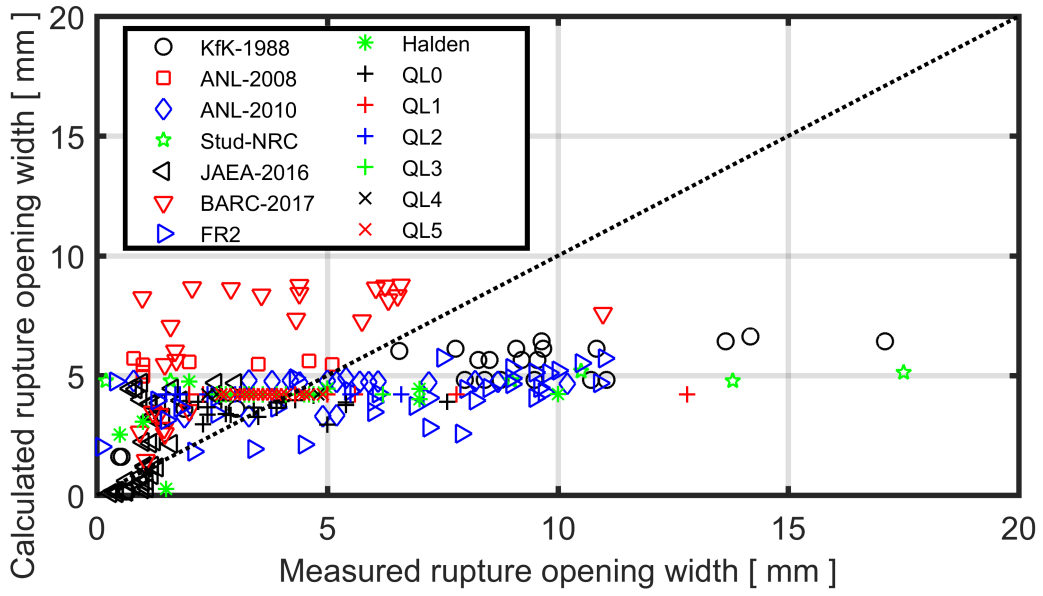

Figure 16: Rupture opening width, calculated through equation 4, in comparison with measured data or estimated values for w_b for each of the 285 tests in the database.

[3] A quantitative measure of the predictability is provided by Pearsons correlation coefficient, which is 0.45 between the calculated and measured values of w_b in Figure 16.

When equation (4) is applied with the best-estimate values for α and β, it bounds 56.8 % of the burst tests in the database, i.e. the calculated value for w_b exceeds the measured or estimated value for 162 of the 285 tests. By increasing α, equation (4) can be transformed from a best-estimate to a more conservative relation for w_b. This is illustrated by Figure 17, which shows the results of equation (4) with α=1.0, σ_{th}=5 MPa and β=3.35$\times 10^{-8}$ Pa^{-1} in comparison with measured and estimated data for w_b. In this case, equation (4) bounds 80.7 % of the burst tests in the database.

In fact, any degree of conservatism can be achieved by modifying α in equation (4), while keeping the best-estimate values for β and σ_{th}. This is clear from Table 3, which shows the percentage of burst tests bounded by equation (4) for different values of α in the range from 1.0 to 1.5. Percentages are presented for the entire database and for the aforementioned two types of data separately.

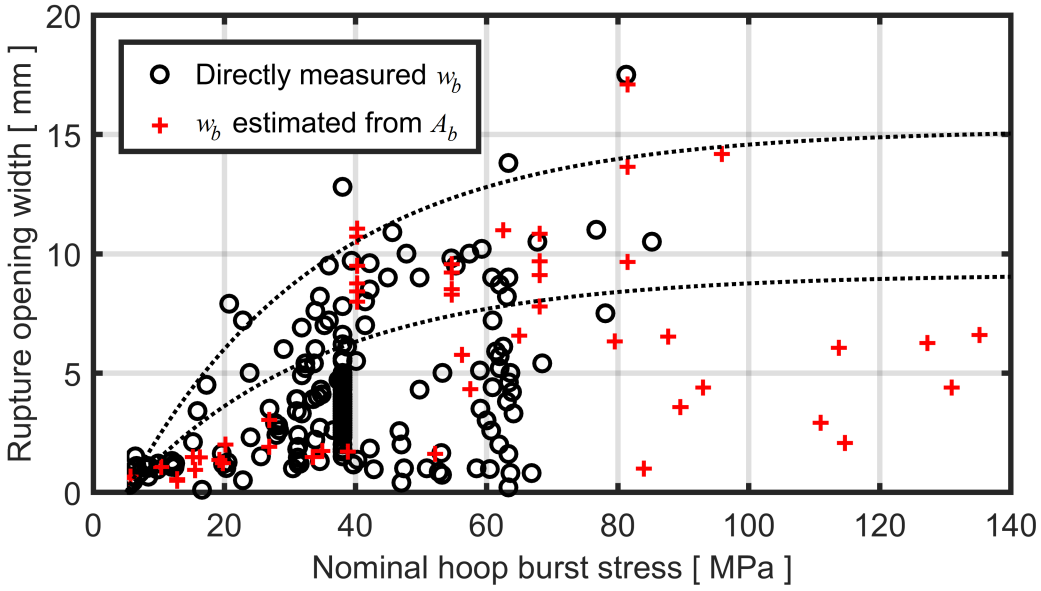

Figure 17: Range of upper bound ($\alpha = 1.0$) rupture opening widths in comparison with the supporting database. Dotted lines correspond to equation (4) with cladding outer diameter D_o=9.13 and 15.20 mm, which is the range spanned by the database. 80.7 % of the 285 burst tests are bounded by the model.

Table 3: Percentage of burst tests bounded by equation (4) with different values for parameter α. For comparison, α=0.5848 is the best-estimate value with regard to the total database.

α [−]	Total database (285 tests)	Measured w_b (235 tests)	Estimated w_b (50 tests)
1.0	80.7	81.3	78.0
1.1	86.7	87.2	84.0
1.2	90.2	91.1	86.0
1.3	93.0	93.2	92.0
1.4	95.1	95.3	94.0
1.5	95.4	95.7	94.0
0.5848	56.8	57.0	56.0

Equation (4) provides a simple correlation for estimating the circumferential width of the cladding rupture opening. The calculation can be done with a suitable degree of conservatism by modifying parameter α, and the results put forth in Table 3 provide the information needed for setting α. Once w_b has been calculated from equation (4), the axial length and area of the rupture opening may be estimated through equations (2) and (3).

Finally, although available data suggest that there are differences between different types of zirconium base cladding materials regarding their rupture opening dimensions under LOCA, and that effects of irradiation and cladding corrosion may exist, the current database is insufficient to quantify these differences and effects. The models provided by equations (2)-(4) are considered to be applicable to Zircaloy, M5 and ZIRLO cladding materials in un-irradiated as well as irradiated state.

4 Summary, conclusions and outlook

4.1 Summary and conclusions

An extensive database, comprising eight experiment series with totally 164 burst tests on single fuel rods under simulated LOCA conditions and six bundle tests with altogether 121 failed rods, was compiled and analysed with regard to the reported size and shape of the breach in the ruptured cladding. These two types of tests complement each other: In single rod tests, the boundary conditions for the tested rod can be better controlled and monitored than in bundle tests. On the other hand, bundle tests are probably more representative for the true accident conditions, since they reproduce rod-to-rod interaction and gradients in temperature and other properties across the fuel rod bundle.

All tests in the considered database were conducted on fuel rods with zirconium alloy cladding in steam environment, with sufficient steam supply to feed the high-temperature metal-water reactions without steam starvation. Most of the tests were done out-of-reactor on as-fabricated or hydrogen-charged cladding materials, but 44 tests were done in-reactor on UO_2 light-water-reactor fuel rods with fuel pellet burnups up to about 90 MWd(kgU)$^{-1}$.

The data for rupture opening dimensions in the considered database exhibit a spread that is considerably larger than for other rupture properties, such as the cladding rupture stress and strain. Systematic differences between test series may be explained by differences in heating methods and heating rates used in the experiments, leading to various degrees of circumferential and axial gradients in cladding temperature, and hence, to various degrees of localization of cladding deformation. However, there is a large spread in data also within test series, where testing conditions are nominally identical for all samples. This spread is attributed mainly to random deviations from axial symmetry of the cladding samples, e.g. from geometrical imperfections or unintended circumferential temperature gradients.

Analysis of the data with regard to rupture opening shape showed that the cladding breach is typically somewhere between the shape of a rhombus and an ellipse. Moreover, with regard to its length-to-width ratio, l_b/w_b, the breach changes from crack-like ($l_b/w_b > 10$) for small breaches to mouth-like ($l_b/w_b \approx 2$) for large rupture openings. We noted that the rupture opening width w_b is usually less than the cladding as-fabricated outer diameter. Based on the analysis, correlations were formulated that relate fundamental rupture opening dimensions (area, axial length, circumferential width) to each other.

From the analysis of the database with regard to rupture opening shape, we concluded that the circumferential width is the limiting dimensional parameter that will determine whether fuel pellet fragments of a given size may be ejected through the cladding breach. For this reason, we focussed the analysis on the width of the rupture opening, and a correlation was proposed, by which the width can be calculated from the as-fabricated dimensions of the cladding tube and the internal overpressure at time of burst. The correlation is formulated such that it may serve either as a best-estimate model or as a conservatively bounding model: the degree of conservatism (percentage of tests in the database bounded by the model) can be conveniently set by varying a single model parameter. Considering the large spread in rupture opening data, it can be expected that the model will be applied in bounding rather than best-estimate mode.

The proposed empirical model is considered to be applicable to Zircaloy, M5 and ZIRLO cladding materials in un-irradiated as well as irradiated state. It is different from existing empirical models for the cladding rupture opening in that it focusses on the circumferential width rather than the area of the breach. Once the width has been calculated, the axial length and area of the rupture opening may be estimated through the relations derived from our analysis of the database.

4.2 Outlook

The empirical models for cladding rupture opening dimensions developed in this report will be implemented in the FRAPTRAN-QT-1.5 computer program, where they will be linked to computational models for fuel pellet gas-induced fragmentation and axial relocation that were developed in earlier LOCA-related research projects for SSM. By comparing the calculated rupture opening dimensions with the calculated amount and size distribution of axially relocatable fuel fragments, it will be possible to estimate the amount of fuel material that may be dispersed into the primary coolant from a failed fuel rod.

In this context, it should be remarked that the fuel rod internal overpressure is expected to affect the fuel dispersal in two different ways: through the cladding rupture opening dimensions (related to the magnitude of the local overpressure at time of cladding burst) and through the propensity for fuel fragment ejection (related to the magnitude and duration of axial pressure gradients after burst that may entrain fuel fragments in the flowing gas). While the first effect of rod internal overpressure is considered by the models developed in this report, the second effect has to be considered by a separate model for axial flow of gas within the fuel rod.

The models developed in this report do not discriminate between different types of zirconium base cladding materials, nor do they account for possible changes in rupture opening formation in the materials as a result of in-reactor operation. Available data suggest that there are differences between different types of zirconium base cladding materials regarding their rupture opening dimensions under LOCA. For example, in the QUENCH-LOCA series of bundle tests, the rupture opening width was on average 26 % lower for M5 cladding than for Zircaloy-4 under nominally identical testing conditions, and data from burst tests on Optimized ZIRLO cladding fell between these two alloys. These differences were observed for as-fabricated cladding materials, and it is not clear whether they persist during in-reactor operation: as of today, there are very few burst tests conducted on irradiated cladding materials other than Zircaloy-4. Hence, in order to formulate material-specific models for the rupture opening, applicable to irradiated material, further LOCA simulation tests are needed on M5 and ZIRLO cladding materials in irradiated condition.

Further tests are also needed to investigate possible effects of cladding hydrogen content on the rupture opening dimensions. The current database includes a handful of experiments on hydrogen-charged materials. The results from these experiments are consistent in that they show a reduction in cladding burst temperature with increasing hydrogen concentration. However, the results are conflicting regarding the effect of hydrogen on rupture opening size.

Acknowledgements

The work was funded by the Swedish Radiation Safety Authority (SSM) under research contract number SSM 2018-4296. Anna Alvestav at SSM is gratefully acknowledged for initiating the project and for providing helpful feedback to the work.

References

[1] B. Pershagen. *Light water reactor safety*. Pergamon Press, Oxford, England, 1989.

[2] Nuclear fuel behaviour in loss-of-coolant (LOCA) conditions. Report NEA No. 6846, OECD Nuclear Energy Agency, Paris, France, 2009.

[3] W. Wiesenack. Summary of the Halden Reactor Project LOCA test series IFA-650. Report HPR-380, Institutt for Energiteknikk, Halden, Norway, 2013.

[4] M. E. Flanagan, P. Askeljung, and A. Puranen. Post-test examination results from integral, high-burnup, fueled LOCA tests at Studsvik Nuclear Laboratory. Report NUREG-2160, U.S. Nuclear Regulatory Commission, Washington, DC, USA, 2013.

[5] Report on fuel fragmentation, relocation, dispersal. Report NEA/CSNI/R(2016)16, OECD Nuclear Energy Agency, Paris, France, 2016.

[6] P. A. C. Raynaud. Fuel fragmentation, relocation and dispersal during the loss-of-coolant accident. Report NUREG-2121, U.S. Nuclear Regulatory Commission, Washington, DC, USA, 2012.

[7] K. J. Geelhood, W.G. Luscher, and J. M. Cuta. FRAPTRAN-1.5: A computer code for the transient analysis of oxide fuel rods. Report NUREC/CR-7023, Vol.1 Rev.1, U.S. Nuclear Regulatory Commission, Washington, DC, USA, 2014.

[8] A. R. Massih and L. O. Jernkvist. Assessment of data and criteria for cladding burst in loss-of-coolant accidents. Research report 2015:46, Swedish Radiation Safety Authority, Stockholm, Sweden, 2015.

[9] L. O. Jernkvist and A. R. Massih. Calibration of models for cladding tube high-temperature creep and rupture in the FRAPTRAN-QT-1.5 program. Technical Report TR20-003, Quantum Technologies AB, 2020.

[10] L. O. Jernkvist. A review of analytical criteria for fission gas induced fragmentation of oxide fuel in accident conditions. *Progress in Nuclear Energy*, 119:103188, 2020.

[11] J. A. Turnbull, S. K. Yagnik, M. Hirai, D. M. Staicu, and C. T. Walker. An assessment of the fuel pulverization threshold during LOCA-type temperature transients. *J. Nucl. Sci. Engng.*, 179:477–485, 2015.

[12] L. O. Jernkvist and A. R. Massih. Models for axial relocation of fragmented and pulverized fuel pellets in distending fuel rods and its effects on fuel rod heat load. Research report 2015:37, Swedish Radiation Safety Authority, Stockholm, Sweden, 2015.

[13] L. O. Jernkvist. Modelling of fine fragmentation and fission gas release of UO_2 fuel in accident conditions. *EPJ Nucl. Sci. Techn.*, 5:11, 2019.

[14] L. O. Jernkvist and A. R. Massih. Improving the FRAPTRAN program for fuel rod LOCA analyses by novel models and assessment of recent data. Annex II, pp 381-

451, IAEA-TECDOC-1889, International Atomic Energy Agency, Vienna, Austria, 2019.

[15] L. O. Jernkvist. Computational assessment of LOCA simulation tests on high burnup fuel rods in Halden and Studsvik. Report 2017:12, Swedish Radiation Safety Authority, Stockholm, Sweden, 2017.

[16] L. O. Jernkvist. Models for axial gas flow and mixing in LWR fuel rods. Research report 2020:02, Swedish Radiation Safety Authority, Stockholm, Sweden, 2020.

[17] M. E. Markiewicz and F. J. Erbacher. Experiments on ballooning in pressurized and transiently heated Zircaloy-4 tubes. Report KfK 4343, Kernforschungszentrum Karlsruhe, Germany, 1988.

[18] F. J. Erbacher, H. J. Neitzel, and K. Wiehr. Cladding deformation and emergency core cooling of a pressurized water reactor in a LOCA: Summary description of the REBEKA program. Report KfK 4781, Kernforschungszentrum Karlsruhe, Germany, 1990.

[19] T. K. Sawarn, S. Banerjee, S. S. Sheelvantra, J. L. Singh, and V. Bhasin. Study of clad ballooning and rupture behaviour of Indian PHWR fuel pins under transient heating condition in steam environment. *J. Nucl. Mater.*, 495:332–342, 2017.

[20] M. Billone, Y. Yan, T. Burtseva, and R. Daum. Cladding embrittlement during postulated loss-of-coolant accidents. Report NUREG/CR-6967, U.S. Nuclear Regulatory Commission, Washington, DC, USA, 2008.

[21] M. C. Billone, Y. Yan, T. A. Burtseva, and R. O. Meyer. Cladding embrittlement during postulated loss-of-coolant accidents. Report NUREG/CR-7219, U.S. Nuclear Regulatory Commission, Washington, DC, USA, 2016.

[22] T. Narukawa and M. Amaya. The effect of oxidation and chrystal phase condition on the ballooning and rupture behavior of Zircaloy-4 cladding tube under transient heating conditions. *J. Nucl. Sci. Techn.*, 53(1):112–122, 2016.

[23] E. H. Karb, L. Sepold, P. Hofmann, C. Petersen, G. Schanz, and H. Zimmermann. LWR fuel rod behavior during reactor tests under loss-of-coolant conditions: Results of the FR2 in-pile tests. *J. Nucl. Mater.*, 107:55–77, 1982.

[24] E. H. Karb, M. Prüßmann, L. Sepold, P. Hofmann, and G. Schanz. LWR fuel rod behavior in the FR2 in-pile tests simulating the heatup phase of a LOCA. Report KfK 3346, Kernforschungszentrum Karlsruhe, Germany, 1983.

[25] J. Stuckert, M. Grosse, C. Rössger, M. Steinbrück, and M. Walter. Results of the commissioning test QUENCH-L0 performed under LOCA conditions. Scientific report SR-7571, Karlsruher Institut für Technologie, Karlsruhe, Germany, 2018.

[26] J. Stuckert, M. Grosse, M. Steinbrück, M. Walter, and A. Wensauer. Results of the QUENCH-LOCA experimental program at KIT. *J. Nucl. Mater.*, 534:Paper 152143, 2020.

[27] J. Stuckert, M. Grosse, C. Rössger, M. Steinbrück, and M. Walter. Results of the reference bundle test QUENCH-L1 with Zircaloy-4 claddings performed under LOCA

conditions. Scientific report SR-7651, Karlsruher Institut für Technologie, Karlsruhe, Germany, 2018.

[28] J. Stuckert, M. Grosse, C. Rössger, M. Steinbrück, and M. Walter. Results of the LOCA bundle test QUENCH-L2 with M5 claddings. Scientific report SR-7677, Karlsruher Institut für Technologie, Karlsruhe, Germany, 2018.

[29] J. Stuckert, M. Grosse, C. Rössger, M. Steinbrück, and M. Walter. Results of the LOCA bundle test QUENCH-L3 with optimised ZIRLO claddings. Scientific report SR-7737, Karlsruher Institut für Technologie, Karlsruhe, Germany, 2018.

[30] J. Stuckert, M. Grosse, , A. Pshenichnikov, C. Rössger, M. Steinbrück, and M. Walter. Results of the LOCA bundle test QUENCH-L4 with pre-hydrogenated M5 claddings. Scientific report SR-7712, Karlsruher Institut für Technologie, Karlsruhe, Germany, 2018.

[31] J. Stuckert, M. Grosse, C. Rössger, M. Steinbrück, and M. Walter. Results of the LOCA bundle test QUENCH-L5 with pre-hydrogenated optimised ZIRLO claddings. Scientific report SR-7738, Karlsruher Institut für Technologie, Karlsruhe, Germany, 2018.

[32] J. M. Kramer and L. W. Deitrich. Cladding failure by local plastic instability. In *Fourth International Conference on Structural Mechanics in Reactor Technology (SMiRT-4)*, volume C, San Francisco, CA, USA, August 15-19, 1977. Paper C 3/12.

[33] F. J. Erbacher and S. Leistikow. A review of Zircaloy fuel cladding behavior in a loss-of-coolant accident. Report KfK 3973, Kernforschungszentrum Karlsruhe, Germany, 1985.

[34] J. R. Matthews and R. N. Tripp. The ballooning of cladding tubes. *Res Mechanica*, 3:81–94, 1981.

[35] R. S. W. Shewfelt and D. P. Godin. Ballooning of thin-walled tubes with circumferential temperature variations. *Res Mechanica*, 18:21–33, 1986.

[36] P. M. Jones, F. Casadei, and H. Laval. Modelling of azimuthal effects arising from interaction between clad deformation and heat transfer under LB LOCA conditions. *Nucl. Engng. Des.*, 79(3):267–276, 1984.

[37] R. S. W. Shewfelt and D. P. Godin. The effect of axial scratches on the ductile creep rupture of internally pressurized thin-walled tubes. *Res Mechanica*, 13(1), 1985.

[38] L. O. Jernkvist. Prediction of failure of highly irradiated Zircaloy clad tubes under reactivity initiated accidents. In *Seventeenth International Conference on Structural Mechanics in Reactor Technology (SMiRT-17)*, volume C, Prague, Czech Republic, August 17-22, 2003. Paper C03-4.

[39] T. Narukawa and M. Amaya. The effect of azimuthal temperature distribution on the ballooning and rupture behavior of Zircaloy-4 cladding tube under transient heating conditions. *J. Nucl. Sci. Techn.*, 53(11):1758–1765, 2016.

[40] S. Suman. Influence of hydrogen concentration on burst parameters of Zircaloy-4 cladding tube under simulated loss-of-coolant accident. *Nucl. Engng. and Techn.*, 52(9):2047–2053, 2020.

[41] A. R. Massih and L. O. Jernkvist. Modeling alpha-beta phase transformation kinetics in Zr-base alloys. Memo PM19-008V2, Quantum Technologies AB, Uppsala, Sweden, 2019.

[42] A. R. Massih and L. O. Jernkvist. Solid state phase transformation kinetics in Zr-base alloys. *Scientific Reports*, 2020. (submitted).

[43] J. C. Brachet, L. Portier, and T. Forgeron. Influence of hydrogen content on the α/β phase transformation temperatures and on the thermal-mechanical behavior of Zy-4, M4 (ZrSnFeV), and M5$^{\mathrm{TM}}$ (ZrNbO) alloys during the first phase of LOCA transient. In G. D. Moan and P. Rudling, editors, *Zirconium in the Nuclear Industry: Thirteenth International Symposium*, volume ASTM STP 1423, pages 673–701, West Conshohocken, PA, USA, 2002. American Society for Testing and Materials.

[44] H. M. Chung and T. F. Kassner. Deformation characteristics of Zircaloy cladding in vacuum and steam under transient-heating conditions: Summary report. Report NUREG-CR-0344, U.S. Nuclear Regulatory Commission, Washington, DC, USA, 1978.

[45] J. A. Nelder and R. Mead. A simplex method for function minimization. *Computer Journal*, 7(4):308–313, 1965.

[46] MATLAB Optimization Toolbox. Manual, The Mathworks, Natick, MA, USA, 2016.

[47] K. Wiehr and H. Schmidt. Out-of-pile experiments on ballooning of Zircaloy fuel rod claddings: Test results with shortened fuel rod simulators. Report KfK 2345, Kernforschungszentrum Karlsruhe, Germany, 1977.

[48] Y. Yan, R. V. Strain, and M. C. Billone. LOCA research results for high-burnup BWR fuel. In *Proceedings of the 2002 Nuclear Safety Research Conference*, volume NUREG/CP-0180, pages 127–155, Washington, DC, USA, 2002. U.S. Nuclear Regulatory Commission.

[49] Y. Yan, T. A. Burtseva, R. O. Meyer, and M. C. Billone. Update of LOCA-integral and post-LOCA-bend test results for fresh ZIRLO cladding. Argonne National Laboratory letter report to U.S. Nuclear Regulatory Commission, July 2010. U.S. NRC ADAMS Accession No. ML111380437.

[50] Y. Yan, T.A. Burtseva, R. O. Meyer, and M. C. Billone. Argonne results for ANL-Studsvik benchmark tests. Argonne National Laboratory letter report to U.S. Nuclear Regulatory Commission, August 2010. U.S. NRC ADAMS Accession No. ML111380445.

[51] M. C. Billone. Assessment of current test methods for post-LOCA cladding behavior. Report NUREG/CR-7139, U.S. Nuclear Regulatory Commission, Washington, DC, USA, 2012.

[52] M. E. Flanagan. Mechanical behavior of ballooned and ruptured cladding. Report NUREG-2119, U.S. Nuclear Regulatory Commission, Washington, DC, USA, 2012.

[53] E. Kolstad, W. Wiesenack, B. Oberländer, and T. Tverberg. High burnup fuel behaviour under LOCA conditions as observed in Halden reactor exepriments. In *Fuel Behaviour and Modelling Under Severe Transient and Loss of Coolant Acci-*

dent (LOCA) Conditions, IAEA-TECDOC-CD-1709, pages 207–218, Vienna, Austria, 2013. International Atomic Energy Agency.

A Experimental data

A.1 Definitions

The hoop burst strain presented throughout this report is permanent (residual) engineering strain, defined by

$$\varepsilon_b = \Delta L / L_o, \tag{A.1}$$

where ΔL is the permanent increase of the cladding tube perimeter[4] from an initial perimeter L_o. The circumferential burst opening w_b is excluded from ΔL, which means that ε_b is the (axial peak, circumferential average) permanent hoop strain experienced by the cladding material at time of burst.

The hoop burst stress presented in this report is the *nominal* stress, i.e. it is calculated without considering the changes in cladding geometry (increase in average radius and decrease in wall thickness) caused by the ballooning. It is the average value across the wall thickness, calculated from the overpressure at time of burst, ΔP_b, and the cladding as-fabricated dimensions through the well-known equation for thin-walled tubes

$$\sigma_b = \Delta P_b \frac{R_o}{W_o}, \tag{A.2}$$

where R_o and W_o are the as-fabricated (un-deformed) cladding average radius and wall thickness. We note that $R_o = (R_{coo} + R_{cio})/2$ and $W_o = R_{coo} - R_{cio}$, where R_{cio} and R_{coo} are the as-fabricated inner and outer radii of the cladding tube.

Burst test data from the experiment series considered in this report are presented in the following. The tables have a common format, where the columns contain the following data:

1. Test sample name/identifier/label, ID (-)
2. Heating rate, $\dot{T}$ (Ks^{-1})
3. Sample initial overpressure at pre-transient temperature, ΔP_o (MPa)
4. Sample overpressure at time of burst, ΔP_b (MPa)
5. Cladding temperature at burst, T_b (K)
6. Engineering hoop strain at burst, ε_b (-)
7. Nominal hoop stress at burst, σ_b (MPa)
8. Max circumferential width of the rupture opening, w_b (mm)
9. Axial length of the rupture opening, l_b (mm)
10. Area of the rupture opening, A_b (mm^2)

It should be remarked that the literature sources do not always contain all these data for each and every test sample: this is commented in the subsections below.

[4]Maximum value with regard to axial position along the sample.

A.2 Data from single rod tests

A.2.1 KfK-1988 test series

The KfK-1988 test series comprises out-of-reactor burst tests with transient heating, conducted on fresh Zircaloy-4 cladding in steam atmosphere in the REBEKA test facility, Kernforschungszentrum Karlsruhe, Germany [17, 18]. The material in these tests was PHWR Zircaloy-4 cladding, produced by two different manufacturers: CONVAR (C) in Argentina and NRG (N) in Germany. The main purpose of the tests was to compare the LOCA behaviour of the cladding materials produced by these two suppliers. As-fabricated cladding samples were heated from inside by use of electrical resistance heaters with a heating length of 325 mm. In addition, the samples were heated from outside by a shroud electrical heater. This created a near-uniform temperature distribution in the samples: the temperature differences along the cladding circumference were less than 10 K [17]. The heating was slow, to simulate the expected LOCA conditions in a PHWR. All samples had a nominal outer diameter of 11.90 mm and a wall thickness of 0.550 mm. The total internal gas volume of the samples was 25 cm^3, with about 9 cm^3 in an upper plenum volume and 16 cm^3 in a lower plenum [47].

Data for the measured burst opening area are reported graphically versus burst temperature in Fig. 9 of [17]. Only part of the data points in this figure can be unambiguously linked to specific tests, which means that only 25 of totally 41 tests can be used in our assessment of rupture opening dimensions. No data are provided for the width and length of the rupture opening.

The measured rupture opening areas are plotted versus burst temperature in Figure A.1 and versus hoop burst stress in Figure A.2. From Figure A.2, it is clear that a nominal hoop burst stress of at least 40 MPa is needed for achieving large rupture openings. From Table A.1, it is also clear that large rupture openings are reported only for samples with hoop burst strain in excess of about 60 %.

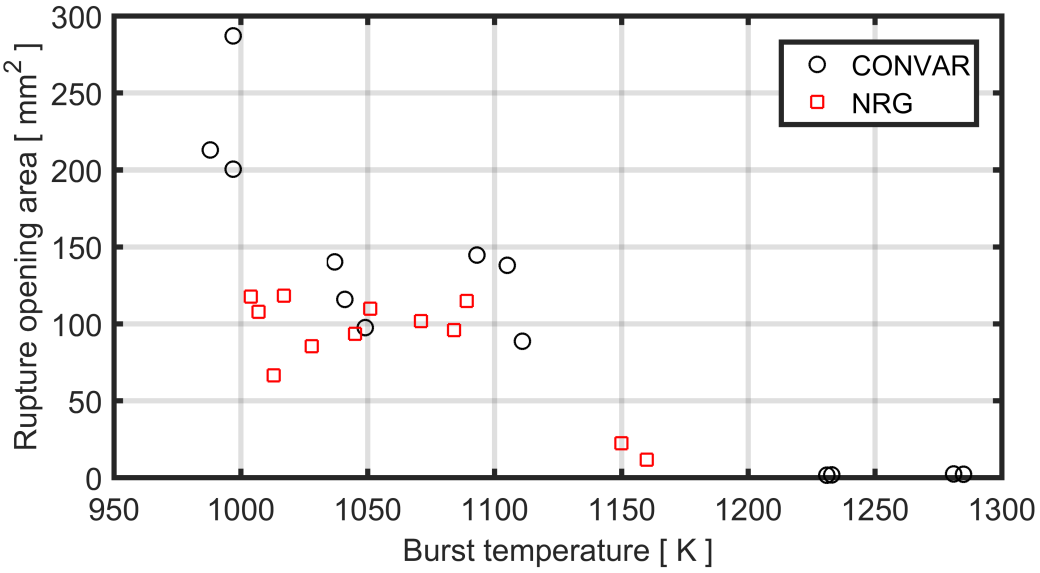

Figure A.1: Measured rupture opening area, A_b, versus burst temperature, T_b, for the KfK-1988 test samples.

Table A.1: Data from the KfK-1988 burst test series on Zircaloy-4 CONVAR (C) and NRG (N) samples [17, 18].

Test ID	$\dot{T}$ [Ks^{-1}]	ΔP_o [MPa]	ΔP_b [MPa]	T_b [K]	ε_b [%]	σ_b [MPa]	w_b [mm]	l_b [mm]	A_b [mm^2]
C1	1.08	3.9	3.9	1105	84	40.24	-	-	137.9
C2	1.08	3.9	3.9	1093	70	40.24	-	-	144.5
C3	1.08	3.9	3.9	1111	106	40.24	-	-	88.6
C4	1.08	5.3	5.3	1049	99	54.69	-	-	97.5
C5	1.08	5.3	5.3	1041	76	54.69	-	-	115.8
C8	1.08	6.6	6.6	1037	85	68.10	-	-	140.1
C10	1.08	7.9	7.9	997	74	81.51	-	-	200.4
C12	1.08	7.9	7.9	997	76	81.51	-	-	287.1
C14	1.08	9.3	9.3	988	78	95.96	-	-	212.9
C39	1.08	1.24	1.24	1231	68	12.79	-	-	1.41
C40	1.08	1.24	1.24	1233	56	12.79	-	-	1.71
C41	1.08	0.55	0.55	1285	26	5.67	-	-	2.05
C42	1.08	0.55	0.55	1281	24	5.67	-	-	2.33
N1	1.08	3.9	3.9	1084	73	40.24	-	-	95.8
N2	1.08	3.9	3.9	1071	82	40.24	-	-	101.6
N3	1.08	3.9	3.9	1089	88	40.24	-	-	114.7
N4	1.08	5.3	5.3	1051	93	54.69	-	-	109.7
N6	1.08	5.3	5.3	1045	69	54.69	-	-	93.5
N7	1.08	6.3	6.3	1013	67	65.00	-	-	66.5
N8	1.08	6.6	6.6	1028	72	68.10	-	-	85.3
N9	1.08	6.6	6.6	1017	76	68.10	-	-	118.1
N10	1.08	6.6	6.6	1007	77	68.10	-	-	107.6
N11	1.08	7.9	7.9	1004	79	81.51	-	-	117.5
N17	1.08	2.6	2.6	1150	60	26.83	-	-	22.2
N18	1.08	2.6	2.6	1160	63	26.83	-	-	11.5

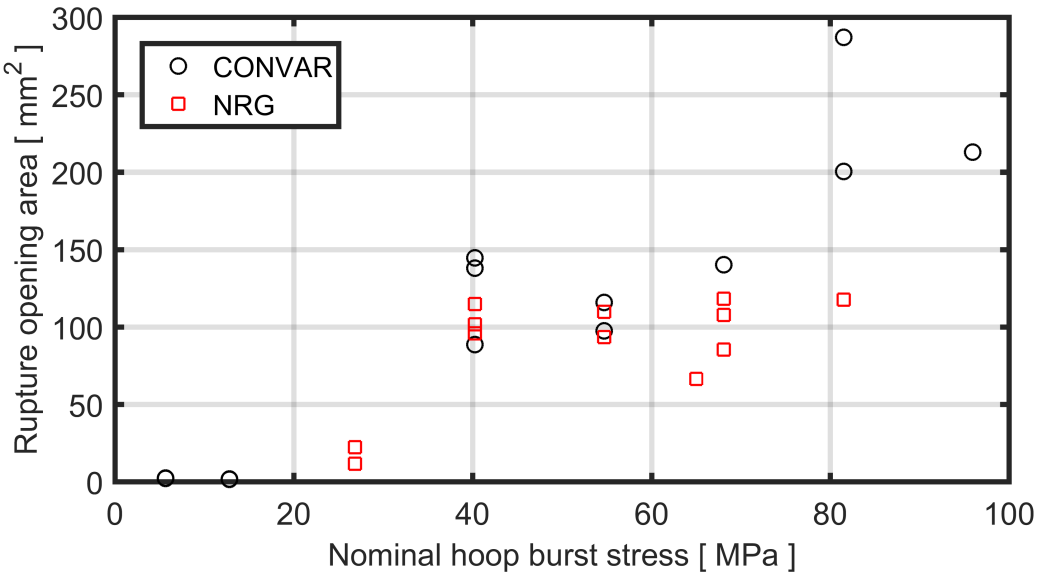

Figure A.2: Measured rupture opening area, A_b, versus nominal hoop burst stress, σ_b, for the KfK-1988 test samples.

A.2.2 ANL-2008 test series

The considered ANL-2008 tests comprise 8 out-of-reactor burst tests on Zircaloy-2 (Zr-1.5Sn-0.2Fe-0.1Cr-0.05Ni by wt%) cladding material, carried out in steam at the Argonne National Laboratory (ANL), USA [20, 48]. The material was commercial cladding material with internal zirconium liner, used for 9×9-type BWR fuel. The cladding outer diameter was 11.18 mm and the wall thickness 0.71 mm. The samples were 300 mm long and the internal gas volume, including connected pressure lines, was 10 cm^3 [48]. Five of the considered tests were done outside the hot-cell (OCL-series) on un-irradiated (as-fabricated) cladding material, whereas three tests were done in the hot-cell (ICL-series) on samples taken from discharged fuel rods with an average burnup of 56-57 $MWd(kgU)^{-1}$. These samples were moderately corroded, with an external oxide layer of about 10 μm and a hydrogen concentration around 70 wppm [20]. All tests were done under identical conditions to allow comparisons between the samples: they were brought to an initial temperature of 573 K, pressurized to 8.28 MPa and then heated to burst with a constant heating rate of 5 Ks^{-1}. The internal pressure varied moderately during the test, due to gradually increasing sample temperature and internal volume. External heating was used.

The measured rupture opening widths are plotted versus burst temperature in Figure A.3 and versus hoop burst stress in Figure A.4. The un-irradiated (OCL) samples have exceptionally narrow burst openings, while the openings of pre-irradiated (ICL) samples are comparable to those reported from other studies. The OCL samples have l_b/w_b-ratios around 10, which means that the rupture openings are crack-like.

Table A.2: Data from the ANL-2008 burst test series on un-irradiated (OCL) and pre-irradiated (ICL) Zircaloy-2 samples [20, 48].

Test ID	$\dot{T}$ [Ks^{-1}]	ΔP_o [MPa]	ΔP_b [MPa]	T_b [K]	ε_b [%]	σ_b [MPa]	w_b [mm]	l_b [mm]	A_b [mm^2]
OCL3	5	8.97	8.40	1033	61	61.93	2.0	13	-
OCL11	5	8.28	7.93	1026	43	58.47	1.0	11	-
OCL13	5	8.28	6.43	1039	43	47.41	1.0	10	-
OCL17	5	8.28	9.07	1023	49	66.87	0.8	10	-
OCL22	5	8.28	6.90	1020	54	50.87	1.0	17	-
ICL2	5	8.28	8.01	1023	39	59.06	3.5	14	-
ICL3	5	8.28	8.60	1003	43	63.41	4.6	11	-
ICL4	5	8.28	8.00	1063	36	58.99	5.1	15	-

A.2.3 ANL-2010 test series

The ANL-2010 tests considered here comprise 19 out-of-reactor burst tests on un-irradiated ZIRLO cladding material of the first generation (Zr-1.0Sn-1.0Nb-0.1Fe by wt%), carried out in steam at ANL. Measured rupture opening dimensions are reported for 13 samples that were tested in as-fabricated condition and 6 samples that were tested after being gaseously charged with 220 - 700 wppm hydrogen.

The tests are partially described in many sources [21, 49–52], and the reported results are not always consistent from one source to another. The results presented here are taken

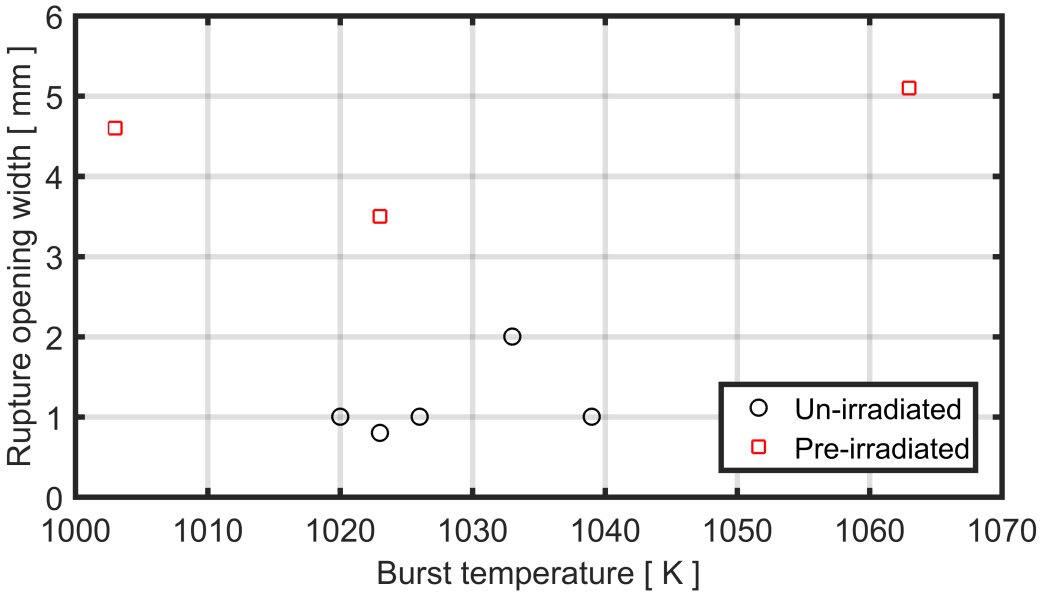

Figure A.3: Measured rupture opening width, w_b, versus burst temperature, T_b, for the ANL-2008 test samples.

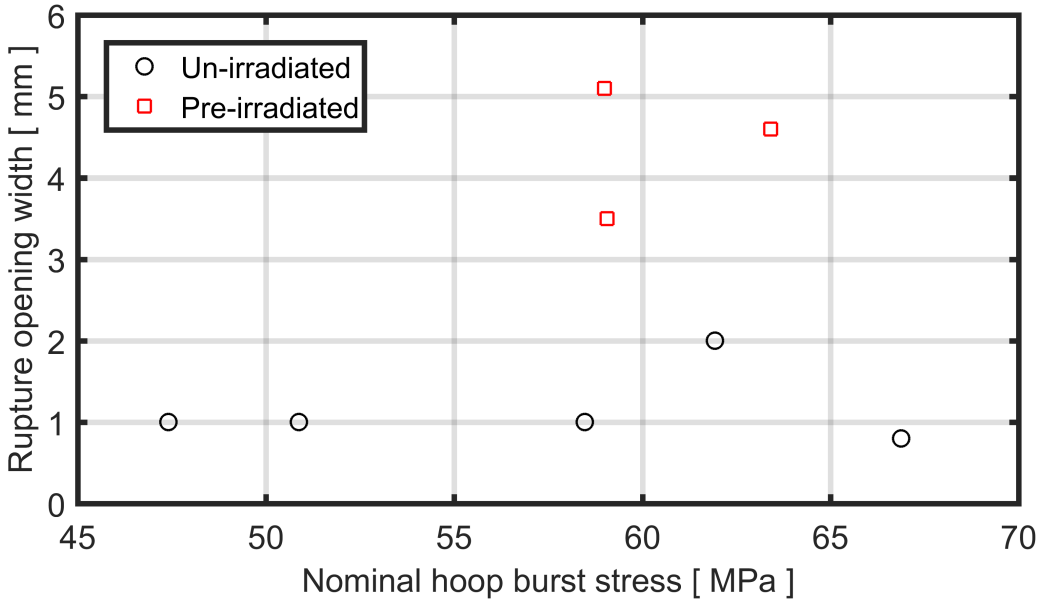

Figure A.4: Measured rupture opening width, w_b, versus nominal hoop burst stress, σ_b, for the ANL-2008 test samples.

from the last, and hopefully the most correct, report [21]. The tested material was ZIRLO cladding of 17×17-type PWR fuel rod design, with an outer diameter of 9.50 mm and a wall thickness of 0.571 mm. The total gas volume in the sample and connected pressure lines was 10 cm^3, and most of the gas was outside the heated zone. The testing conditions were very similar to those used previously by ANL, as described in Section A.2.2 above.

The measured rupture opening widths are plotted versus burst temperature in Figure A.5. It is clear that the burst temperature is generally lower for the hydrogen-charged samples. This result is consistent with the findings from the QUENCH-LOCA bundle tests, where as-fabricated versus hydrogen-charged cladding materials were compared; see Section A.3. Figure A.5 also suggests that the burst opening width tend to be somewhat lower for the hydrogen-charged samples, but this trend is fairly weak. In fact, a recent experimental study on ballooning and burst of hydrogen-charged samples of Zircaloy-4 cladding in inert (argon) atmosphere rather than steam showed that the rupture opening was larger in hydrogen-charged samples than in as-fabricated samples [40]. We also note that the results for ε_b shown in Table A.3 follows a trend that is opposite to that of w_b: the hydrogen-charged samples tend to have larger burst strains than the as-fabricated samples.

The measured rupture opening widths are plotted versus hoop burst stress in Figure A.6. There are only four tests at low stress, but the trend is clear: high burst stress is a necessary but not sufficient condition for getting wide rupture openings.

Table A.3: Data from the ANL-2010 burst test series on as-fabricated and hydrogen-charged ZIRLO cladding samples [21].

Test ID	$\dot{T}$ [Ks^{-1}]	ΔP_o [MPa]	ΔP_b [MPa]	T_b [K]	ε_b [%]	σ_b [MPa]	w_b [mm]	l_b [mm]	A_b [mm^2]
Samples in as-fabricated condition									
14	5	8.27	8.07	1008	48	63.10	3.8	11.0	-
15	5	8.27	7.79	1028	52	60.91	4.4	18.0	-
17	5	8.27	7.93	1023	45	62.00	5.7	19.0	-
18	5	8.27	8.76	1021	43	68.49	5.4	18.0	-
19	5	4.14	4.07	1113	25	31.82	3.3	12.0	-
21	5	4.14	4.07	1123	28	31.82	4.9	13.0	-
22	5	4.14	4.14	1110	23	32.37	5.2	10.0	-
25	5	8.27	7.93	1030	42	62.00	8.7	26.0	-
29	5	8.27	7.86	1019	49	61.45	5.9	21.0	-
32	5	8.27	7.79	1021	49	60.91	7.2	22.0	-
36	5	8.27	7.58	1023	53	59.27	10.2	24.0	-
37	5	8.27	7.93	1028	46	62.00	5.2	19.0	-
43	5	8.27	8.00	1011	50	62.55	6.1	19.0	-
Samples charged with 220 - 700 wppm hydrogen									
39	5	4.14	4.00	1015	57	31.27	1.9	7.3	-
40	5	8.27	8.17	963	47	63.88	4.2	16.0	-
41	5	8.27	8.20	1003	56	64.11	3.3	15.0	-
42	5	8.27	8.14	955	71	63.64	0.8	7.5	-
44	5	8.27	8.07	946	56	63.10	8.2	18.0	-
45	5	8.27	8.14	1010	68	63.64	5.0	17.0	-

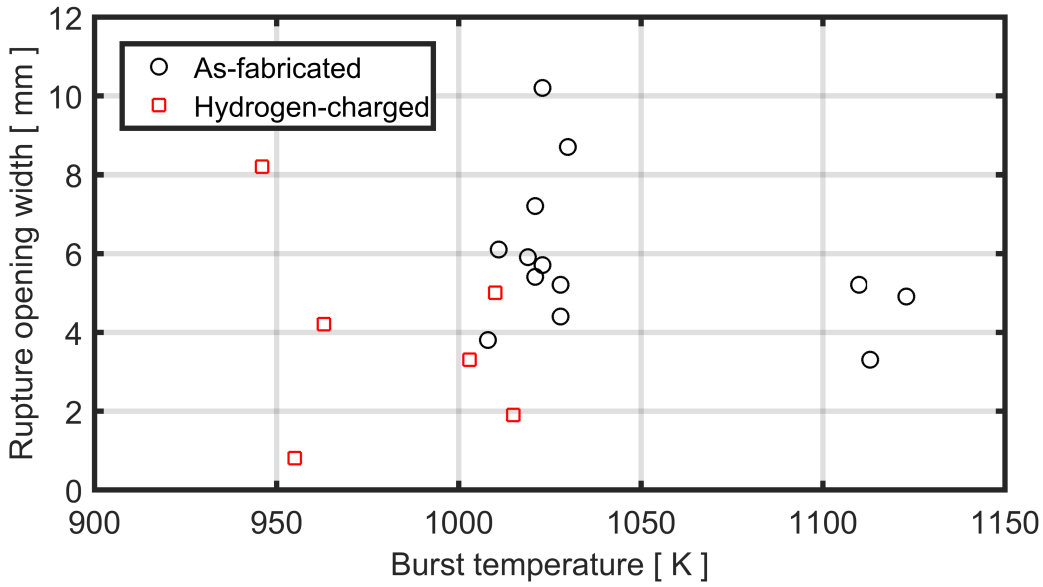

Figure A.5: Measured rupture opening width, w_b, versus burst temperature, T_b, for the ANL-2010 test samples.

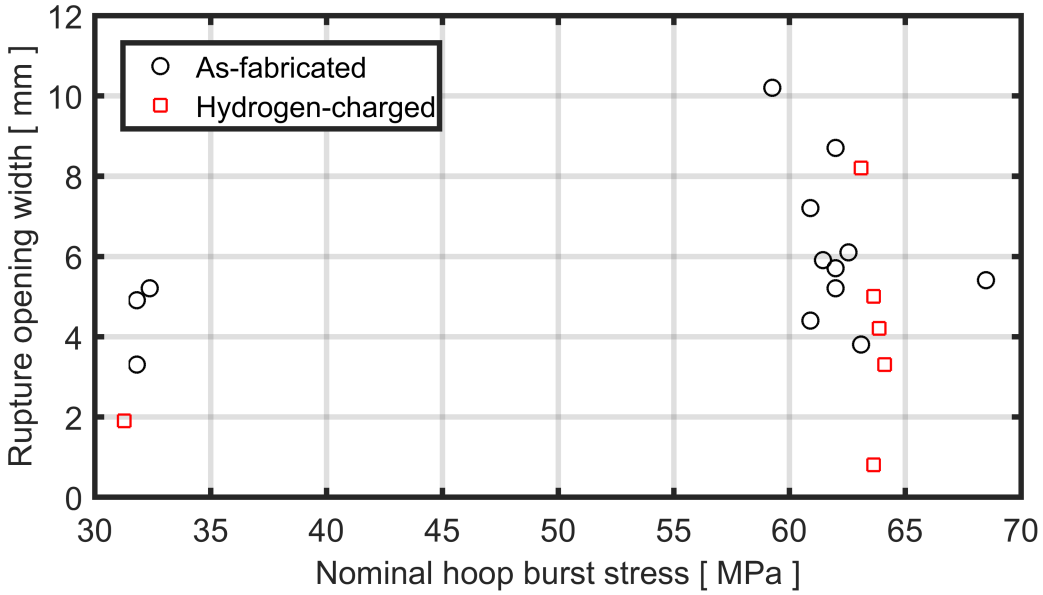

Figure A.6: Measured rupture opening width, w_b, versus nominal hoop burst stress, σ_b, for the ANL-2010 test samples.

A.2.4 Studsvik-NRC test series

The Studsvik-NRC test series includes 6 out-of-reactor burst tests on irradiated ZIRLO cladding material of the first generation, carried out in steam at Studsvik Nuclear, Sweden, under contract with the U.S. Nuclear Regulatory Commission (NRC) [4]. The cladding material was sampled from 17×17-type PWR fuel rods, which had been irradiated to rod average burnups of 55 and 68 MWd(kgU)$^{-1}$. The local burnups for the short-length ($\approx$ 300 mm) samples were estimated to 60 - 78 MWd(kgU)$^{-1}$ [5]. These estimates are given in Table A.4. The cladding tube outer diameter was 9.50 mm and the wall thickness 0.571 mm for all samples. The sample internal gas volume, including pressure lines, was 10.4 cm^3. The cladding samples had an external oxide layer of 20-30 μm and hydrogen concentrations of 150-290 wppm [4]. The testing conditions were very similar to those used by ANL, as described above in Sections A.2.2-A.2.3: the sample initial overpressure in the Studsvik-NRC tests was either 8.2 or 11.0 MPa at 573 K.

The measured rupture opening widths are plotted versus burst temperature in Figure A.7 and versus hoop burst stress in Figure A.8. It is clear from these figures that there is a notable difference in w_b between samples 196/198 and the other four samples. A similar difference exists between the two groups with regard to the hoop burst strain; see Table A.4. Since the fuel burnup differs between the two groups, it is reasonable to believe that the differences in observed w_b and ε_b are caused by differences in the irradiation-induced pre-test state of the cladding material. Moreover, the rupture opening is exceptionally wide for samples 189-193. The length-to-width ratio (l_b/w_b) is 1-3 for these samples, while it is $\approx$7 for samples 196/198.

Table A.4: Data from the Studsvik-NRC burst test series on pre-irradiated ZIRLO samples [4].

Test ID	$\dot{T}$ [Ks^{-1}]	ΔP_o [MPa]	ΔP_b [MPa]	T_b [K]	ε_b [%]	σ_b [MPa]	w_b [mm]	l_b [mm]	A_b [mm^2]	BU [MWd]
189	5	11.0	10.9	973	48	85.22	10.5	23.9	-	72
191	5	11.0	10.4	953	50	81.31	17.5	21.6	-	75
192	5	8.2	8.1	973	56	63.33	9.0	22.7	-	78
193	5	8.2	8.1	1001	50	63.33	13.8	17.8	-	76
196	5	8.2	8.1	959	25	63.33	0.2	1.5	-	61
198	5	8.2	8.1	966	25	63.33	1.6	11.0	-	60

A.2.5 JAEA-2016 test series

The JAEA-2016 test series comprises out-of-reactor burst tests with transient heating, conducted on as-fabricated Zircaloy-4 PWR cladding in steam and argon atmosphere at the Nuclear Safety Research Center, Japan Atomic Energy Agency (JAEA), Tokai-mura, Japan [22]. Here, we consider only the tests done in steam atmosphere. All cladding samples were 190 mm long and had an outer diameter of 9.50 mm and a wall thickness of 0.640 mm. According to information obtained directly from the investigators, the pressurized gas volume in the sample and connected pressure lines was 11 cm^3. The samples were surrounded by an infrared furnace and transiently heated from an initial temperature of 373 K. The tests in steam atmosphere were done with two different heating rates: $\approx$ 3 Ks^{-1} and 25-30 Ks^{-1}.

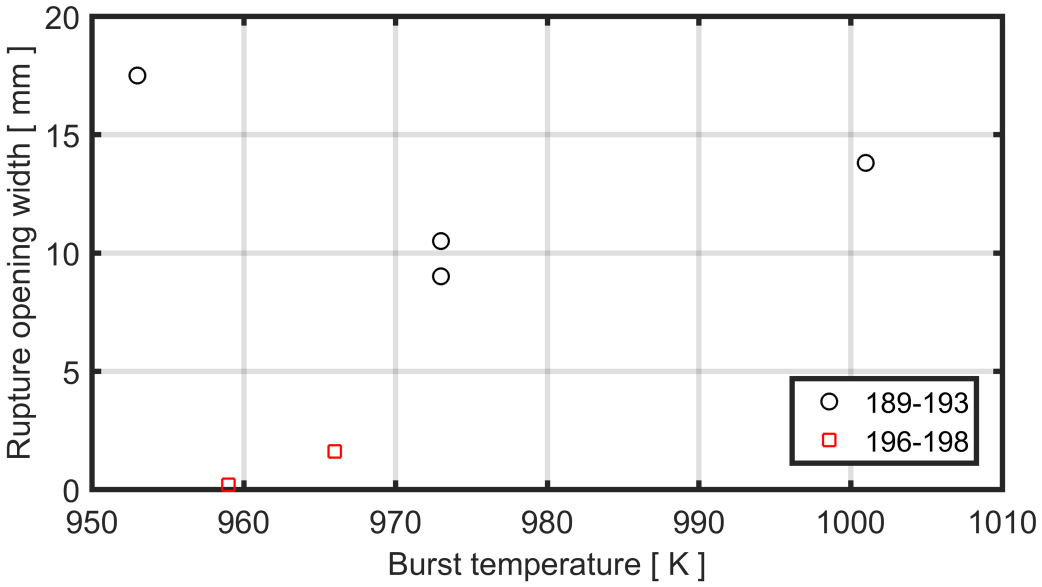

Figure A.7: Measured rupture opening width, w_b, versus burst temperature, T_b, for the Studsvik-NRC test samples.

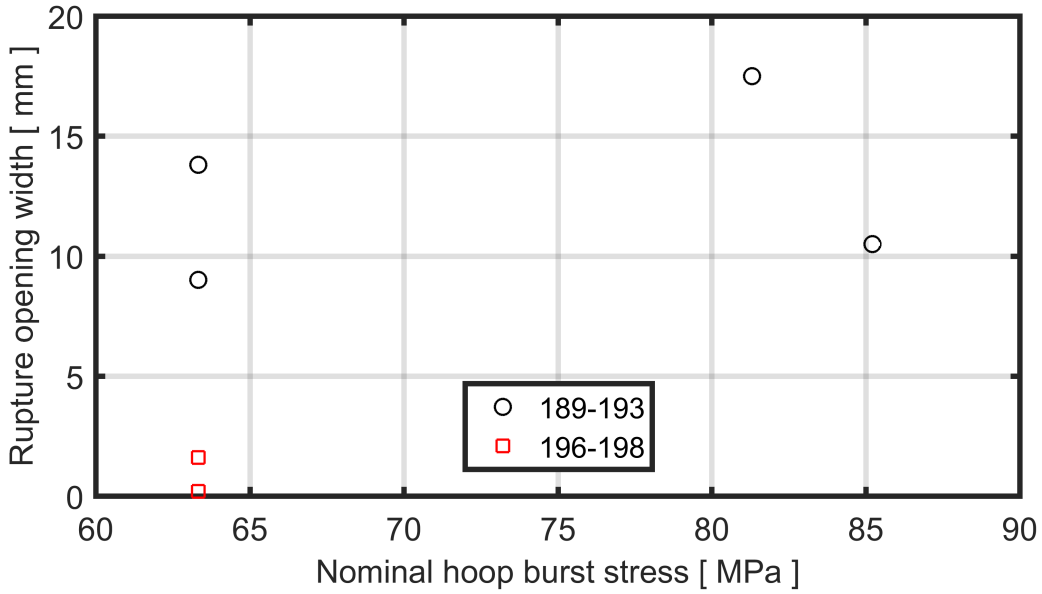

Figure A.8: Measured rupture opening width, w_b, versus nominal hoop burst stress, σ_b, for the Studsvik-NRC test samples.

Table A.5: Data from the JAEA-2016 burst test series on as-fabricated Zircaloy-4 samples [22].

Test ID	$\dot{T}$ [Ks^{-1}]	ΔP_o [MPa]	ΔP_b [MPa]	T_b [K]	ε_b [%]	σ_b [MPa]	w_b [mm]	l_b [mm]	A_b [mm^2]
L1	3	-	8.66	1042	48	60.0	3.01	10.9	26.3
L2	3	-	8.77	1044	39	60.7	2.58	10.5	22.0
L3	3	-	7.67	1066	42	53.1	1.64	9.9	11.4
L4	3	-	6.74	1080	46	46.7	2.56	11.5	21.9
L5	3	-	6.19	1095	31	42.8	0.96	7.3	5.4
L6	3	-	6.10	1097	41	42.2	1.83	12.0	18.3
L7	3	-	5.82	1099	46	40.3	1.36	10.8	12.5
L8	3	-	4.55	1145	28	31.5	1.19	6.8	5.7
L9	3	-	4.53	1150	25	31.3	1.18	6.3	4.9
L10	3	-	2.96	1176	15	20.5	1.25	6.3	5.1
L11	3	-	2.93	1192	18	20.3	1.01	6.4	5.0
L12	3	-	1.81	1223	20	12.5	1.21	5.1	4.3
L13	3	-	1.79	1232	36	12.4	1.05	4.9	3.5
L14	3	-	1.22	1257	32	8.5	1.09	5.5	3.0
L15	3	-	1.21	1267	33	8.4	0.65	3.9	1.9
L16	3	-	1.03	1291	44	7.1	0.81	2.4	1.5
L17	3	-	0.88	1380	19	6.1	0.45	2.8	0.8
L18	3	-	0.79	1423	10	5.5	0.30	3.1	0.7
L19	3	-	0.80	1463	10	5.5	0.44	4.8	1.1
H1	25	-	8.74	1081	18	60.5	0.97	5.5	3.7
H2	25	-	7.69	1112	19	53.2	0.73	3.5	1.8
H3	25	-	7.62	1117	15	52.7	0.85	5.2	2.9
H4	25	-	5.72	1124	16	39.6	1.18	5.0	4.1
H5	25	-	5.74	1139	17	39.7	1.16	6.0	4.8
H6	25	-	1.74	1147	21	12.0	1.31	4.1	3.6
H7	25	-	2.86	1192	15	19.8	1.17	4.3	3.7
H8	25	-	4.51	1204	10	31.2	1.28	5.7	5.1
H9	25	-	1.74	1213	25	12.0	1.06	3.2	2.5
H10	25	-	2.83	1221	15	19.6	1.62	6.4	6.8
H11	25	-	4.51	1231	13	31.2	1.45	4.3	4.8
H12	25	-	1.41	1268	32	9.8	0.95	4.9	3.5
H13	25	-	1.18	1297	26	8.2	1.01	3.4	2.2
H14	25	-	1.43	1367	22	9.9	1.20	4.5	3.6
H15	25	-	0.92	1424	23	6.4	1.00	4.9	3.1
H16	25	-	1.17	1432	39	8.1	1.01	5.4	4.0
H17	25	-	0.95	1440	39	6.6	1.10	7.9	6.5
H18	25	-	0.84	1582	31	5.8	0.65	2.2	1.0

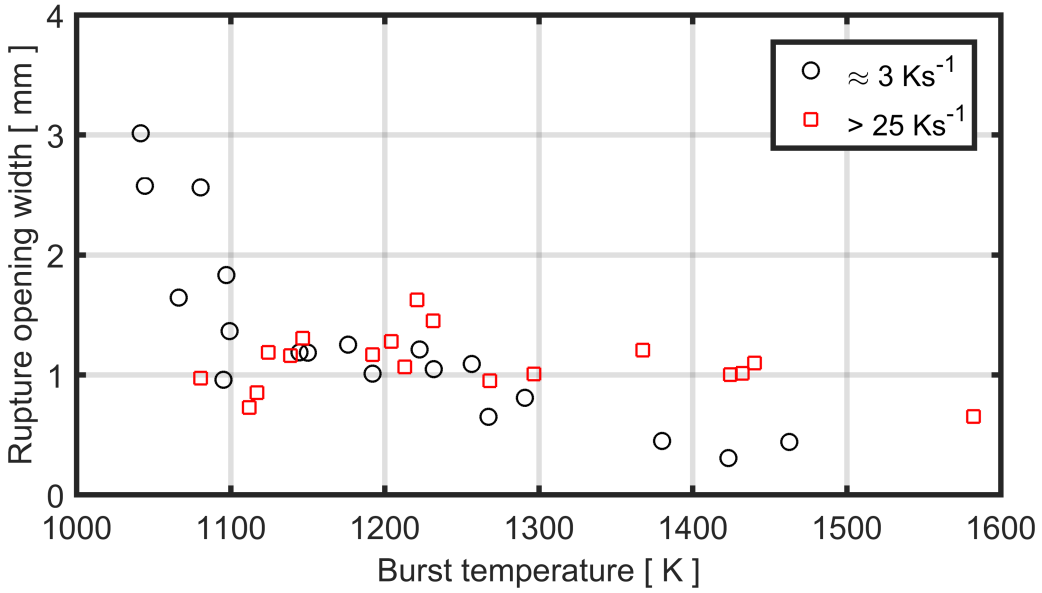

Figure A.9: Measured rupture opening width, w_b, versus burst temperature, T_b, for the JAEA-2016 test samples.

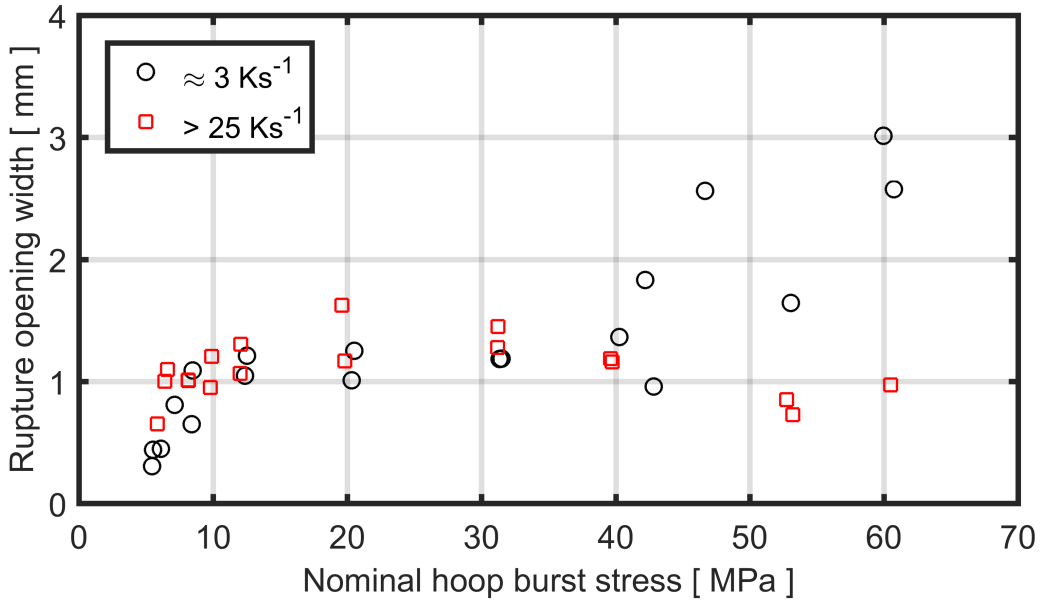

Figure A.10: Measured rupture opening width, w_b, versus nominal hoop burst stress, σ_b, for the JAEA-2016 test samples.

In [22], results are presented in graphical form. The data set is large and contains measured values for all rupture opening dimensions, i.e. w_b, l_b and A_b. Since the graphs have high resolution, they have been digitized with fairly high accuracy: the digitized results are presented in Table A.5. Please note that these digitized values may depart somewhat (<0.5 %) from numerical values presented in the running text of [22].

The measured rupture opening widths are plotted versus burst temperature in Figure A.9 and versus hoop burst stress in Figure A.10. It is clear from these figures that the rupture openings are comparatively narrow in this test series: compare for example with the rupture openings reported from the ANL-2010, FR2 and QUENCH-LOCA test series. Possible explanations to the unexpectedly small rupture openings have been discussed by the investigators in a companion paper [39]. These explanations include circumferential and axial temperature gradients in the samples, possibly leading to localized cladding deformation and burst.

Figure A.9 shows that wide rupture openings are observed only in slowly heated samples that have failed at low temperature. These samples experience a nominal hoop stress in excess of 40 MPa, as shown in Figure A.10. From the latter figure, it is also clear that the rupture opening width tends to very small values (<1 mm), when the nominal hoop burst stress is lower than 10 MPa.

A.2.6 BARC-2017 test series

The BARC-2017 test series comprises out-of-reactor burst tests with transient heating, conducted on as-fabricated Zircaloy-4 PHWR cladding in steam atmosphere at the Bhabha Atomic Research Centre (BARC), Mumbai, India [19]. The cladding samples had an outer diameter of 15.20 mm and a wall thickness of 0.440 mm, which makes them different from samples in other test series considered in this report. Another difference is that direct electrical heating was used in the tests. From graphs of recorded heating histories in [19], it seems that this heating method resulted in significant temperature gradients in the samples, both axially and circumferentially. The pressurized gas volume is reported to be 3 cm^3 in the samples, plus 11 cm^3 in the connected pressure line.

Tests were conducted with a wide spectrum of heating rates and internal overpressures [19]. The rupture opening area, A_b, is reported for 25 samples; see Table A.6. No data are reported for the width or length of the rupture opening, but the rupture shape is reported to change from narrow splits with sharp V-shaped ends at low overpressure to wider openings with rectangular or broad fish-mouth shape at high pressure. The measured rupture opening areas are plotted versus burst temperature in Figure A.11 and versus hoop burst stress in Figure A.12. From Figure A.12, it is clear that a nominal hoop burst stress of at least 50-60 MPa is needed for achieving large rupture openings.

It should be mentioned that a similar experimental study has been done on hydrogen-charged samples of Zircaloy-4 PHWR cladding. This study is not considered here, because it was conducted in inert (argon) atmosphere rather than steam [40]. However, the study showed that the rupture opening area was larger in hydrogen-charged samples than in as-fabricated samples.

Table A.6: Data from the BARC-2017 burst test series on Zircaloy-4 PHWR cladding samples [19].

Test ID	$\dot{T}$ [Ks^{-1}]	ΔP_o [MPa]	ΔP_b [MPa]	T_b [K]	ε_b [%]	σ_b [MPa]	w_b [mm]	l_b [mm]	A_b [mm^2]
5C	19	0.51	0.56	1252	30.9	10.36	-	-	4.9
8A	14	0.79	0.82	1205	30.1	15.17	-	-	8.0
8B	14	0.81	0.84	1161	23.1	15.54	-	-	4.0
8C	6	0.83	0.88	1135	31.0	16.28	-	-	7.9
10A	14	1.02	1.04	1164	28.9	19.24	-	-	7.0
10B	11	1.03	1.07	1185	22.1	19.79	-	-	6.0
10C	5	1.08	1.09	1166	23.1	20.16	-	-	12.4
20A	9	2.03	1.89	1141	15.3	34.96	-	-	10.0
20B	8	1.99	1.81	1143	38.2	33.48	-	-	8.0
20C	14	2.03	2.10	1101	20.7	38.85	-	-	9.8
30A	15	2.98	2.82	1125	32.2	52.17	-	-	9.0
30B	16	3.16	3.04	1073	28.7	56.24	-	-	55.0
30C	7	3.16	3.11	1077	44.6	57.53	-	-	36.7
40A	11	4.22	3.38	1047	66.2	62.53	-	-	143.0
40B	11	4.17	4.30	1013	67.7	79.55	-	-	63.0
40C	10	4.18	4.54	1014	37.3	83.99	-	-	4.4
50A	14	5.01	4.84	984	42.7	89.54	-	-	28.0
50B	14	5.07	4.74	1042	62.7	87.69	-	-	66.0
50C	14	5.04	5.03	959	60.4	93.05	-	-	37.5
60A	18	6.13	6.00	913	26.7	111.00	-	-	21.0
60B	17	6.04	6.20	907	33.3	114.70	-	-	13.0
60C	17	6.20	6.15	921	32.2	113.78	-	-	59.2
70A	15	7.16	7.31	899	24.0	135.23	-	-	67.0
70B	17	7.02	6.88	871	23.1	127.28	-	-	62.0
70C	18	7.10	7.08	916	32.2	130.98	-	-	37.5

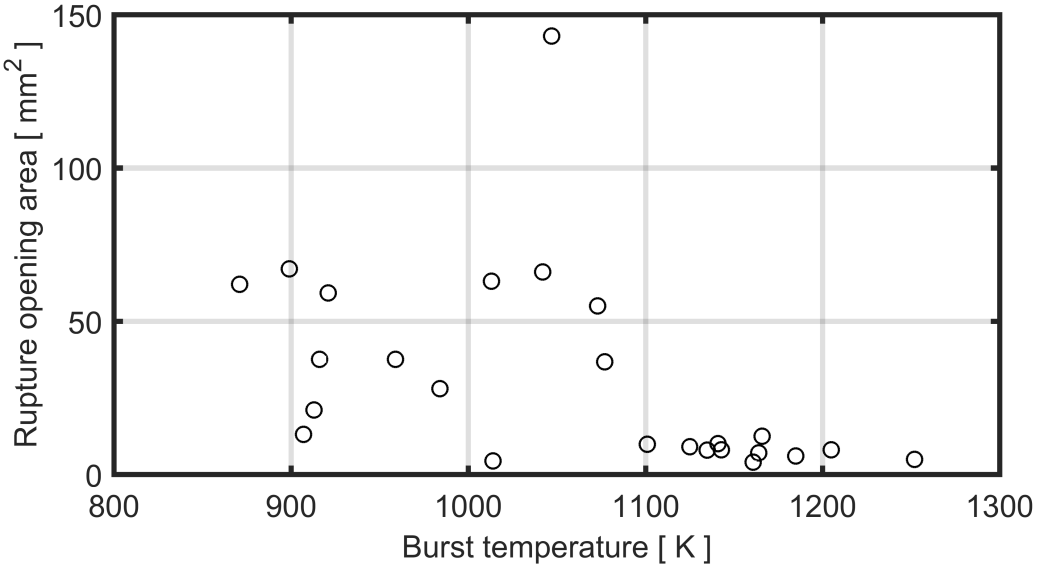

Figure A.11: Measured rupture opening area, A_b, versus burst temperature, T_b, for the BARC-2017 test samples.

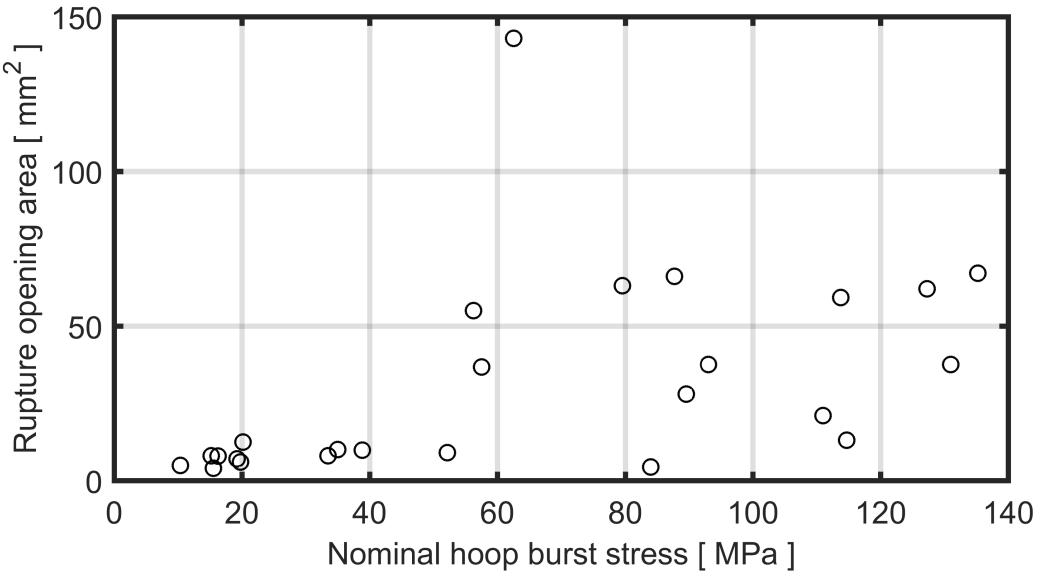

Figure A.12: Measured rupture opening area, A_b, versus nominal hoop burst stress, σ_b, for the BARC-2017 test samples.

A.2.7 FR2 test series

The FR2 test series includes in-reactor burst tests conducted on fresh and pre-irradiated test fuel rods with Zircaloy-4 cladding in the FR2 research reactor, Germany [23, 24]. The test rods considered here were charged with UO_2 fuel pellets and heated by nuclear fission reactions in the pellets. The pre-irradiated rods were operated to burnups from 2.6 to 36.5 MWd(kgU)$^{-1}$ in the FR2 before LOCA testing. The cladding tube dimensions were identical for all rods: the cladding had an outer diameter of 10.75 mm and a wall thickness of 0.725 mm. The heated length was around 500 mm for all test rods and the internal gas volume ranged from 30.0 to 30.8 cm^3. This fairly large internal volume is comparable to that of commercial, full-length fuel rods used in German PWRs during the 1980s. The exact initial cladding temperature for individual tests is not reported. Based on the data presented for selected tests, the initial temperature has been assumed to be 600 K for all tests. The heating rates given below are calculated from this assumption and the burst times and burst temperatures reported for each test.

It should be noticed that the pre-irradiation conditions in the FR2 research reactor were significantly different from the conditions in a commercial PWR. For example, the coolant inlet temperature and pressure was about 330 K and 0.2 MPa, respectively, which means that the cladding corrosion was negligible even for the 36.5 MWd(kgU)$^{-1}$ test rods. Moreover, the FR2 was operated in 40-day cycles, interrupted by shutdowns that lasted for 10-15 days [23, 24].

The measured rupture opening widths are plotted versus burst temperature in Figure A.13 and versus hoop burst stress in Figure A.14. In both figures, data for un-irradiated (fresh) and pre-irradiated samples are interspersed, suggesting that the irradiation has no significant effects on the cladding burst opening. Figure A.14 shows that the rupture opening width correlates with the nominal hoop burst stress. This result is in line with the findings from other studies assessed in this report, but it seems that the threshold stress for creation of wide rupture openings is lower for the FR2 test rods than for cladding samples in

most other studies. This could possibly be an effect of the exceptionally large internal gas volume (≈30 cm^3) in the FR2 test rods.

The l_b/w_b-ratio of the rupture opening is typically 3-4 for $\Delta P_b > 7$ MPa, but it may reach much higher values for lower pressures. This is consistent with findings from other studies, see e.g. Section A.2.6.

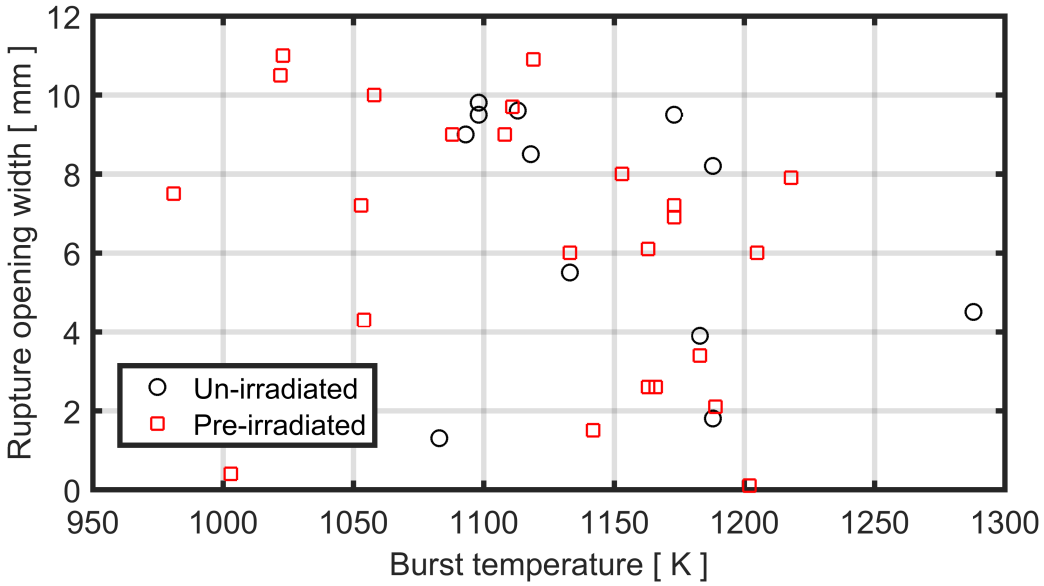

Figure A.13: Measured rupture opening width, w_b, versus burst temperature, T_b, for the FR2 test rods.

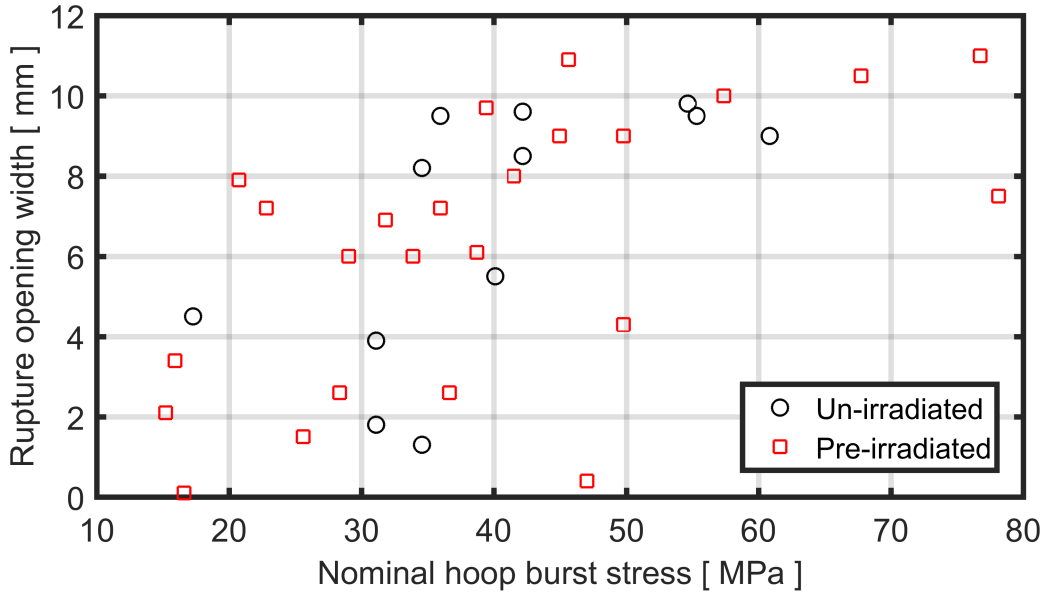

Figure A.14: Measured rupture opening width, w_b, versus nominal hoop burst stress, σ_b, for the FR2 test rods.

Table A.7: Data from the FR2 burst test series on fresh and pre-irradiated UO_2 fuel rods with Zircaloy-4 cladding [23, 24].

Test ID	$\dot{T}$ [Ks^{-1}]	ΔP_o [MPa]	ΔP_b [MPa]	T_b [K]	ε_b [%]	σ_b [MPa]	w_b [mm]	l_b [mm]	A_b [mm^2]
Fresh (un-irradiated) test rods									
A1.1	6.0	5.2	5.0	1083	64.0	34.57	1.3	19	-
A2.1	24.5	9.4	8.8	1093	36.2	60.84	9.0	35	-
A2.2	13.9	6.7	5.8	1133	56.3	40.10	5.5	50	-
A2.3	12.4	2.6	2.5	1288	34.7	17.28	4.5	19	-
B1.1	14.2	5.6	5.2	1173	29.0	35.95	9.5	41	-
B1.2	8.1	5.0	4.5	1188	25.7	31.11	1.8	11	-
B1.3	13.9	6.6	6.1	1118	34.2	42.17	8.5	36	-
B1.5	8.0	5.2	4.5	1183	60.4	31.11	3.9	45	-
B1.6	8.8	8.5	8.0	1098	38.0	55.31	9.5	28	-
B1.7	12.4	6.6	6.1	1113	34.1	42.17	9.6	49	-
B3.1	10.7	8.5	7.9	1098	36.9	54.62	9.8	27	-
B3.2	10.6	5.6	5.0	1188	49.9	34.57	8.2	33	-
Pre-irradiated test rods with a fuel burnup of 2.6 MWd(kgU)$^{-1}$									
C1	12.1	5.1	4.6	1173	51.2	31.80	6.9	31	-
C2	10.6	3.2	3.0	1218	38.8	20.74	7.9	25	-
C3	13.1	10.5	9.8	1022	36.7	67.75	10.5	33	-
C4	11.8	7.3	6.5	1088	44.4	44.94	9.0	42	-
C5	7.5	2.4	2.2	1189	62.2	15.21	2.1	18	-
Pre-irradiated test rods with a fuel burnup of 8.0 MWd(kgU)$^{-1}$									
E1	9.8	2.5	2.3	1183	30.4	15.90	3.4	13	-
E2	13.0	12.1	11.3	981	46.0	78.13	7.5	17	-
E3	11.2	5.3	4.9	1133	30.9	33.88	6.0	14	-
E4	12.9	7.9	7.2	1054	55.5	49.78	4.3	31	-
E5	8.3	2.3	2.4	1202	67.4	16.59	0.1	6	-
Pre-irradiated test rods with a fuel burnup of 21.9 MWd(kgU)$^{-1}$									
F1	13.0	6.4	5.6	1163	59.0	38.72	6.1	62	-
F2	9.8	5.8	5.3	1166	37.5	36.64	2.6	14	-
F3	10.5	4.4	4.2	1205	27.3	29.04	6.0	20	-
F4	13.6	7.8	7.2	1108	34.1	49.78	9.0	28	-
F5	11.2	6.6	6.0	1153	41.2	41.48	8.0	31	-
Pre-irradiated test rods with a fuel burnup of 33.8 MWd(kgU)$^{-1}$									
G1.2	7.2	7.2	6.8	1003	29.5	47.01	0.4	4	-
G1.3	7.9	4.6	4.1	1163	62.3	28.35	2.6	27	-
G1.4	7.8	8.7	8.3	1058	32.6	57.38	10.0	25	-
G1.5	7.5	5.6	5.2	1053	40.8	35.95	7.2	44	-
Pre-irradiated test rods with a fuel burnup of 36.5 MWd(kgU)$^{-1}$									
G2.1	13.6	-	3.7	1142	31.7	25.58	1.5	6	-
G2.2	16.6	7.1	6.6	1119	28.3	45.63	10.9	33	-
G3.1	12.3	-	3.3	1173	45.7	22.82	7.2	29	-
G3.2	15.4	6.5	5.7	1111	41.4	39.41	9.7	39	-
G3.3	14.5	12.0	11.1	1023	32.4	76.74	11.0	27	-

A.2.8 Halden IFA-650 test series

The IFA-650 series of LOCA simulation tests were conducted from 2003 to 2016 in the Halden heavy water test reactor, Norway. Altogether fifteen tests on short UO_2 fuel rodlets were carried out. Twelve of the tests were made on pre-irradiated fuel rods with high or even very high burnup [3, 53]. In each test, a single test rodlet with an active (fuelled) length of 366-480 mm was instrumented and placed in the centre of the rig, which in turn was placed in one of the experimental channels of the test reactor. The rodlet was surrounded by an electrically heated shroud and a pressure flask. The heated shroud provided boundary conditions that resembled the heating effects of nearby fuel rods with similar power. The heating rate and temperature of the test rodlet was controlled both by nuclear heating of the rodlet itself and the electrical heating of the shroud. The power for the heated shroud was uniformly distributed along the test section, while the axial power profile for the rodlet was peaked to the rodlet midplane.

Here, we consider eight tests for which data on the rupture opening dimensions have been reported. Seven of the UO_2 fuel rodlets used in these tests were sampled from discharged LWR fuel rods of various PWR, BWR and VVER designs. Hence, as shown in Table A.8, the database is heterogeneous with regard to test rodlet design and pre-irradiation conditions.

Table A.8: IFA-650 test rodlet designs and pre-test conditions [3]. LT/DX/LI: Low-tin, Duplex, Liner; Clad OD/WT: As-fabricated outer diameter and wall thickness of the cladding tube; V_g: Rodlet internal gas volume.

Test IFA-	Fuel design	Cladding material	Fuel BU [MWd]	Clad OD [mm]	Clad WT [mm]	V_g [cm^3]	Oxide [μm]	Hydrogen [wppm]
650.2	PWR	Zr-4LT	0	9.50	0.570	17.4	0	10
650.4	PWR	Zr-4DX	92	10.75	0.725	21.5	10	50
650.5	PWR	Zr-4DX	83	10.75	0.725	15.0	75	650
650.7	BWR	Zr-2LI	44	9.62	0.630	17.0	10	44
650.9	PWR	Zr-4DX	90	10.75	0.725	19.0	8	30
650.10	PWR	Zr-4	60	9.50	0.570	17.0	25	185
650.11	VVER	E110	56	9.13	0.680	16.0	5	100
650.12	BWR	Zr-2LI	72	9.62	0.630	1.9	40	300

Testing conditions and key results from the LOCA simulation tests are summarized in Table A.9. The cladding heat-up rate $\dot{T}$ is not well-defined in these tests, since it drops gradually with increasing temperature, typically from 6-12 Ks^{-1} at beginning of the transient to 2-6 Ks^{-1} as the temperature approaches 1000 K. The heating rates presented in Table A.9 pertain to the time of burst. It should also be remarked that the reported rupture opening area, A_b, was estimated from w_b and l_b, assuming either a rhombic shape of the opening, or a rhombus extended with a central rectangular part [3].

The measured rupture opening widths are plotted versus burst temperature in Figure A.15 and versus hoop burst stress in Figure A.16. The latter shows that a nominal hoop burst stress of at least 35 MPa is needed to produce wide rupture openings, which is in line with the results of other studies. From Table A.9, it is clear that rupture openings observed in many of the Halden IFA-650 LOCA simulation tests are exceptionally long: up to 70 mm for the IFA-650.4 test. It is well known from many studies that the length of the rupture

opening correlates with the axial extension of the ballooning part of the fuel rod. This part is generally longer in test setups that create uniform temperature distributions in the cladding, both axially and circumferentially. Just like the KfK-1988 out-of-reactor tests described in section A.2.1, the Halden IFA-650 tests were conducted with a combination of internal and external heating that resulted in uniform cladding temperature, large cladding balloons and rupture openings. The Halden IFA-650 tests are too few for identifying any differences in rupture behaviour between rod designs and/or cladding materials.

Table A.9: Data from the Halden IFA-650 LOCA simulation test series [3].

Test IFA-	$\dot{T}$ [Ks^{-1}]	ΔP_o [MPa]	ΔP_b [MPa]	T_b [K]	ε_b [%]	σ_b [MPa]	w_b [mm]	l_b [mm]	A_b [mm^2]
650.2	5	6.6	6.1	1073	54	47.78	10.0	35	270
650.4	2	6.8	5.1	1053	62	35.26	7.0	70	434
650.5	5	7.4	6.8	1033	15	47.01	2.0	7	7.00
650.7	8	0.9	0.9	1373	23	6.42	1.5	11	8.25
650.9	5	6.8	6.0	1078	61	41.48	7.0	40	224
650.10	2	6.9	6.8	1028	15	53.27	5.0	15	37.5
650.11	5	5.1	4.9	1112	25	30.45	1.0	3	1.50
650.12	2	3.2	3.2	1053	40	22.83	0.5	3	0.75

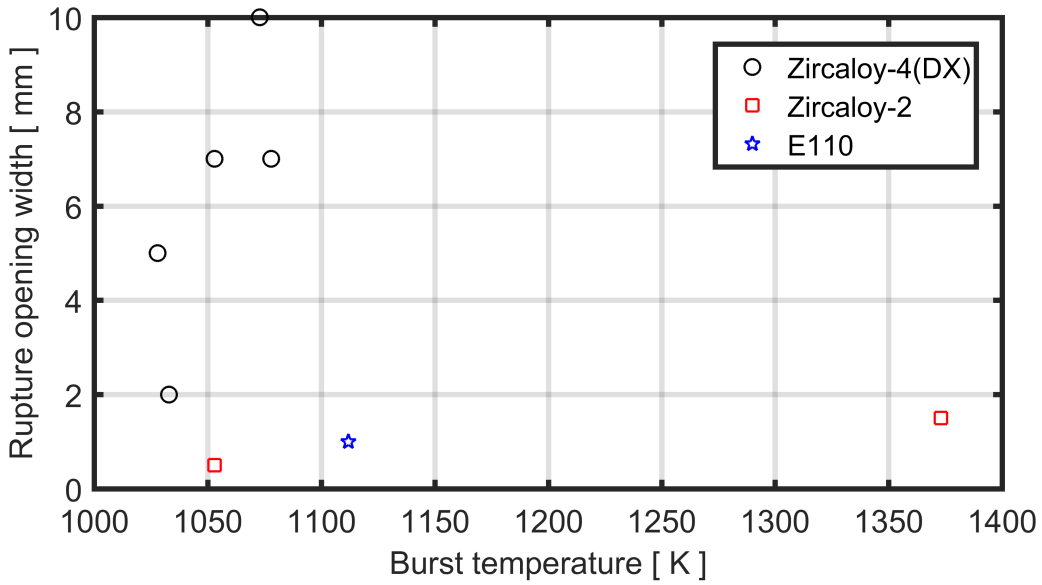

Figure A.15: Measured rupture opening width, w_b, versus burst temperature, T_b, for the Halden IFA-650 test rods.

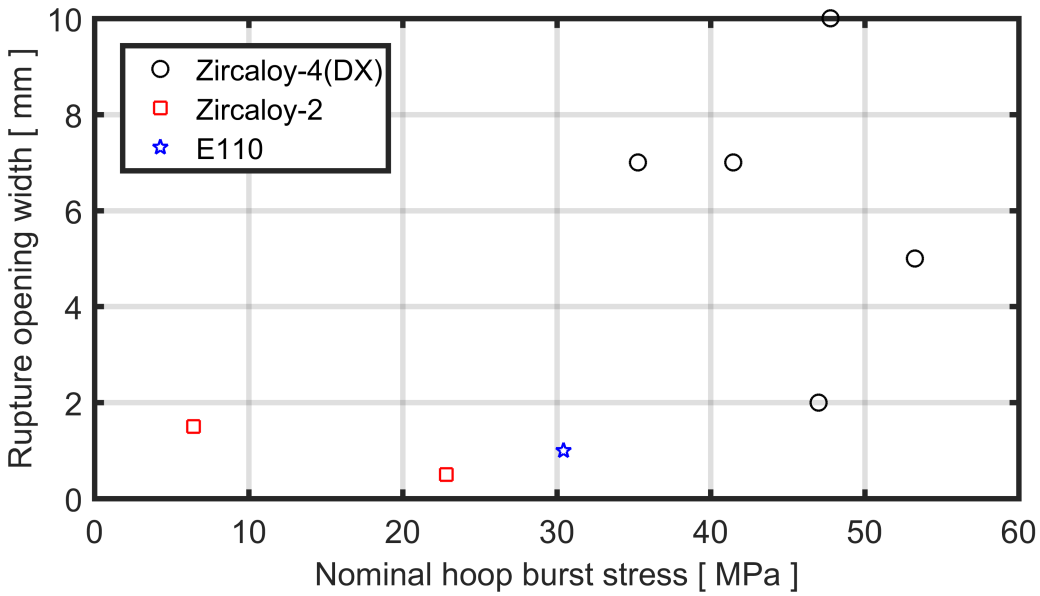

Figure A.16: Measured rupture opening width, w_b, versus nominal hoop burst stress, σ_b, for the Halden IFA-650 test rods.

A.3 Data from bundle tests

The database considered in this report comprises six bundle tests from the QUENCH-LOCA experiment series at Karlsruhe Institute of Technology [26]. As shown in Table 2, the testing conditions are similar in the considered experiments, since they were aimed to reproduce typical conditions in a PWR large-break LOCA. Each bundle comprised 21 electrically heated fuel rod simulators with a total length of about 2.5 m. An internal heater with a length of 1024 mm was used in each rod, and each rod was individually pressurized to a pre-defined overpressure at a pre-test temperature of up to 850 K. All test rods had a free pressurized gas volume, including connected pressure lines, of 31.5 cm^3, to simulate the gas plenum in a full-length PWR fuel rod. Moreover, the cladding tube dimensions were the same for all experiments: the nominal outer diameter was 10.75 mm and the wall thickness 0.725 mm [26].

A.3.1 QL0 test

The QL0 experiment was a commissioning test, carried out under conditions that differed slightly from the subsequent QL1-QL5 experiments. The differences are [25]:

- A lower heating rate for the cladding. It was typically 2-3 Ks^{-1} for the QL0 test, in comparison with 7-8 Ks^{-1} for QL1-QL5;
- No cool-down phase was simulated before terminating the test by water quenching;
- Test rods in the bundle were pressurized to 3.5, 4.0, 4.5, 5.0 or 5.5 MPa.

The system pressure in the QUENCH test loop is 0.3 MPa, which means that the rod internal overpressure at hot pre-test conditions was in the range from 3.2 to 5.2 MPa in the QL0 experiment. For QL1-QL5, a fixed pre-test overpressure of 5.2 MPa was used.

Table A.10 summarizes measured burst parameters for 20 of the 21 test rods in the QL0 bundle: one rod (nr 15) was not overpressurized for reference and did not burst during the test. It should be noticed that the circumferential width of the burst opening, w_b, is not reported in [25]. Here, it has been determined from high-resolution, front-view images of the rupture openings that are presented in [25]. Moreover, the engineering hoop burst strain, ε_b, in Table A.10 is different from that defined in [25]. More precisely, ε_b in Table A.10 is the actual hoop strain of the cladding material and does not include the circumferential deformation contributed by the rupture opening. It is calculated through

$$\varepsilon_b = \tilde{\varepsilon}_b - \varepsilon_{ro} = \tilde{\varepsilon}_b - \frac{w_b}{\pi D_o}, \tag{A.3}$$

where $\tilde{\varepsilon}_b$ is the hoop burst strain reported in [25] and ε_{ro} is the hoop strain corresponding to the circumferential width of the rupture opening. The latter is simply calculated from w_b and the nominal diameter of the cladding tube D_o=10.75 mm.

Table A.10: Data from the QL0 commissioning test on fuel rods with as-fabricated Zircaloy-4 cladding [25]. The rupture opening width, w_b, for each test was determined from high-resolution images in [25].

Test rod	$\dot{T}$ [Ks^{-1}]	ΔP_o [MPa]	ΔP_b [MPa]	T_b [K]	ε_b [%]	σ_b [MPa]	w_b [mm]	l_b [mm]	A_b [mm^2]
1	2.6	4.63	4.55	1069	21.95	33.53	3.9	13.0	36.0
2	2.6	3.08	3.15	1134	18.99	23.85	5.0	12.0	39.7
3	2.6	5.20	5.14	1089	23.08	37.61	4.7	15.0	41.8
4	2.6	4.62	4.65	1073	21.85	34.22	4.0	14.2	35.6
5	2.6	3.50	3.59	1108	16.14	26.89	3.5	11.0	24.0
6	2.6	3.12	3.17	1106	23.99	23.99	2.3	7.6	9.4
7	2.6	5.16	5.11	1066	26.08	37.40	4.7	14.0	40.4
8	2.6	4.47	4.38	1086	33.01	32.36	5.4	17.5	60.4
9	2.6	3.62	3.71	1133	19.41	27.72	2.9	9.0	14.6
10	2.6	4.15	4.22	1064	18.19	31.25	2.4	9.6	13.4
11	2.6	3.68	3.78	1141	20.21	28.21	2.8	10.0	21.9
12	2.6	4.69	4.72	1088	23.77	34.71	4.3	14.5	41.1
13	2.6	4.64	4.60	1078	24.08	33.88	2.2	8.6	12.9
14	2.6	4.60	4.60	1094	25.49	33.88	7.6	18.8	96.5
16	2.6	4.16	4.19	1091	18.13	31.04	3.4	12.0	23.7
17	2.6	3.66	3.74	1127	19.29	27.93	2.4	8.3	12.0
18	2.6	4.60	4.57	1103	18.71	33.67	5.4	17.0	48.1
19	2.6	4.70	4.70	1123	19.20	34.57	2.7	10.3	16.3
20	2.6	4.73	4.74	1049	21.96	34.85	4.1	16.0	53.2
21	2.6	4.14	4.18	1068	14.85	30.97	3.9	15.0	29.2

The rupture opening widths measured for the QL0 and QL1 experiments are plotted versus nominal hoop burst stress in Figure A.17. The stress levels are fairly low in both experiments, and only a minor influence of stress can be seen from the data: from Table 2, it is clear that the average value of w_b is 3.9 mm for QL0 (lower stress) and 4.2 mm for QL1 (higher stress). More significant differences can be seen for the average values of A_b in Table 2: 33.0 mm^2 for QL0 and 47.0 mm^2 for QL1. The rupture opening areas measured for the QL0 and QL1 experiments are plotted versus nominal hoop burst stress in Figure A.18.

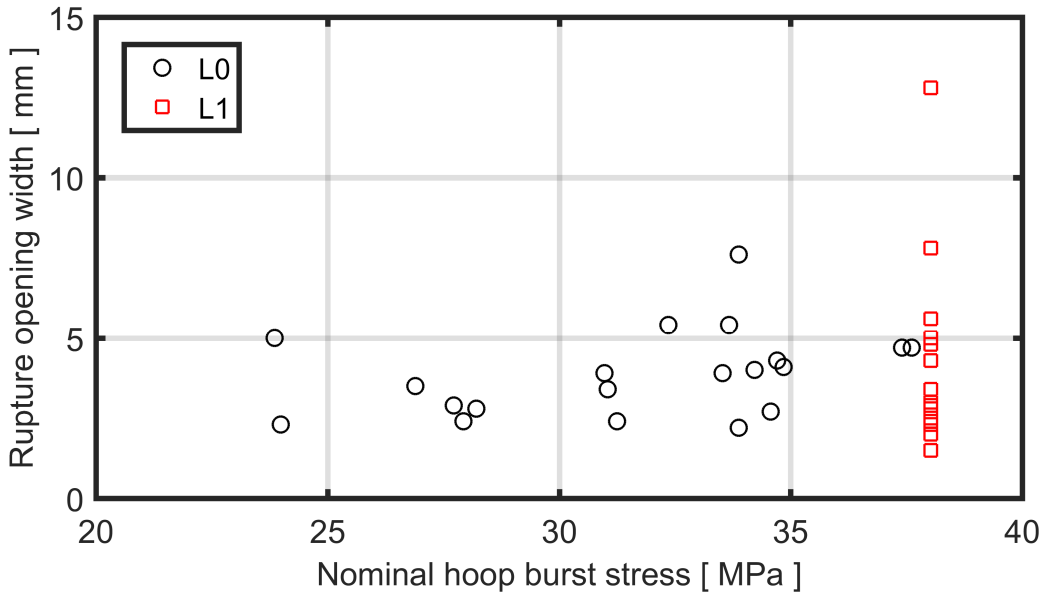

Figure A.17: Measured rupture opening width, w_b, versus nominal hoop burst stress, σ_b, for the QL0 and QL1 test rods (as-fabricated Zircaloy-4 cladding).

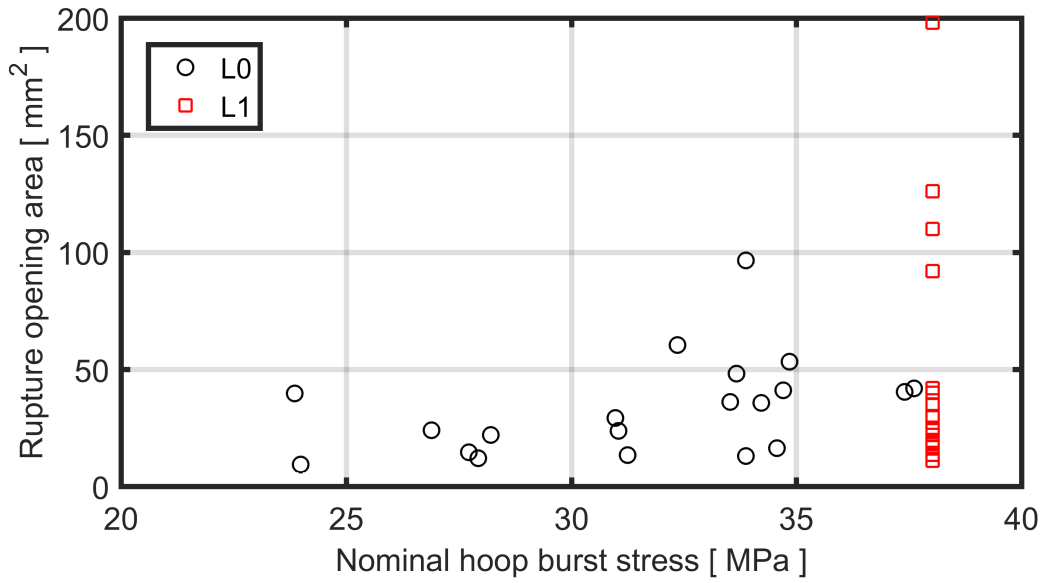

Figure A.18: Measured rupture opening area, A_b, versus nominal hoop burst stress, σ_b, for the QL0 and QL1 test rods (as-fabricated Zircaloy-4 cladding).

A.3.2 QL1 - QL5 tests

Results for individual fuel rods in the QL1 to QL5 bundle tests are compiled in Tables A.11 to A.15. For QL1 and QL4, data are reported only for 19 of the 21 rods in the bundle, since some rods in these two tests failed for other reasons than high-temperature ballooning and burst. As before, the hoop burst strains reported in Tables A.11 to A.15 are calculated through equation (A.3) and therefore different from $\tilde{\varepsilon}_b$ reported in [27]-[31].

All test rods in the QL1-QL5 experiments were pressurized to a hot pre-test internal gas pressure of 5.5 MPa, resulting in an initial overpressure of 5.2 MPa. The internal overpressure at time of cladding burst, ΔP_b, is not reported for individual test rods in [27]-[31]. However, graphs of the pressure histories during the tests show that most rods failed for ΔP_b in the range from 5.0 to 5.4 MPa. Based on this information, it is assumed in our assessment that ΔP_b=5.2 MPa for all test rods in the QL1-QL5 experiments.

A comparison of the burst behaviour of as-fabricated Zircaloy-4, M5 and Optimized ZIRLO cladding is possible by juxtaposing results from the QL1 to QL3 experiments. Figures A.19 and A.20 show the measured rupture opening widths and areas for the three materials in as-fabricated condition. Obviously, Zircaloy-4 has the largest values for w_b and A_b, whereas M5 has the smallest. The difference between the materials is marginal for w_b, but significant for A_b: see the average values presented for w_b and A_b in Table 2.

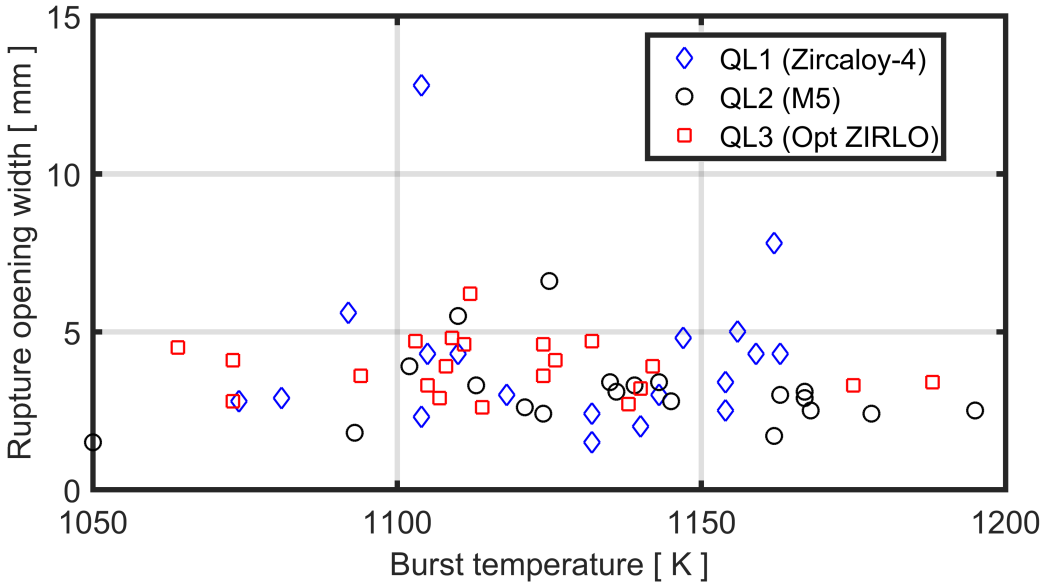

Figure A.19: Measured rupture opening width, w_b, versus burst temperature, T_b, for Zircaloy-4, M5 and Optimized ZIRLO cladding in as-fabricated condition.

The effects of hydrogen on the burst behaviour of un-irradiated cladding materials can be assessed by comparing the results of QL2 versus QL4 for M5 cladding and QL3 versus QL5 for Optimized ZIRLO. For example, the rupture opening widths measured in these two pairs of experiments are shown in Figures A.21 and A.22. As can be seen from these figures and from the average values for the burst parameters in Table 2, the results are very similar for the two materials: The hydrogen has no effect on the rupture opening dimensions w_b, l_b and A_b, but the burst temperature is 30-40 K lower for the hydrogen-charged materials. This decrease in cladding burst temperature is consistent with the effect

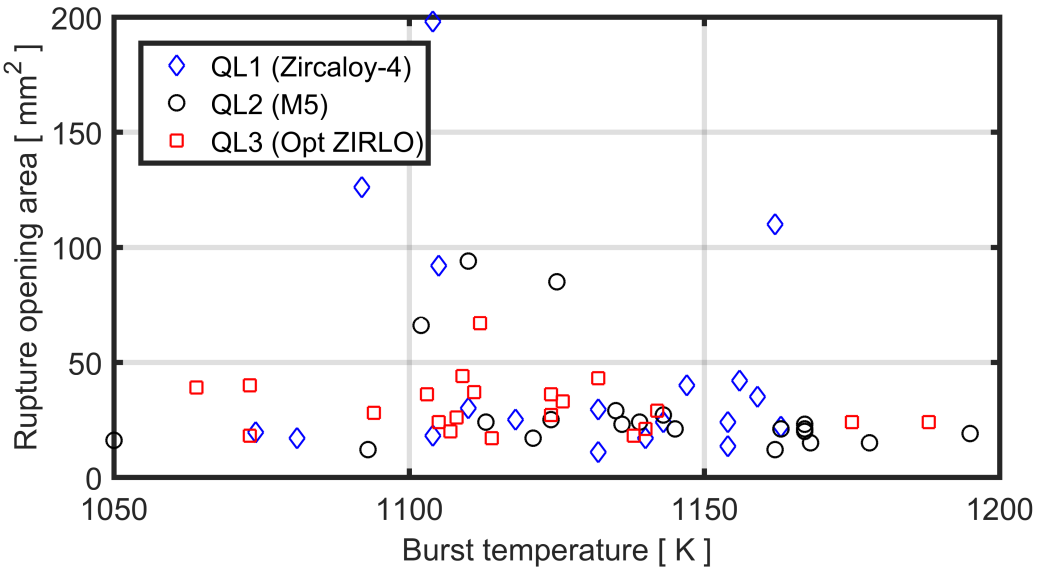

Figure A.20: Measured rupture opening area, A_b, versus burst temperature, T_b, for Zircaloy-4, M5 and Optimized ZIRLO cladding in as-fabricated condition.

Table A.11: Data from the QL1 experiment on fuel rods with as-fabricated Zircaloy-4 cladding [27].

Test rod	$\dot{T}$ [Ks^{-1}]	ΔP_o [MPa]	ΔP_b [MPa]	T_b [K]	ε_b [%]	σ_b [MPa]	w_b [mm]	l_b [mm]	A_b [mm^2]
2	7.5	5.2	5.2	1132	16.59	38.03	2.4	17	29.5
3	7.5	5.2	5.2	1118	27.42	38.03	3.0	13	25.0
4	7.5	5.2	5.2	1154	21.50	38.03	2.5	8	13.5
5	7.5	5.2	5.2	1104	23.10	38.03	12.8	24	198.0
6	7.5	5.2	5.2	1110	21.17	38.03	4.3	12	30.0
7	7.5	5.2	5.2	1074	16.51	38.03	2.8	12	19.5
8	7.5	5.2	5.2	1132	16.86	38.03	1.5	13	11.0
9	7.5	5.2	5.2	1162	17.50	38.03	7.8	20	110.0
10	7.5	5.2	5.2	1143	17.22	38.03	3.0	12	24.0
12	7.5	5.2	5.2	1092	10.92	38.03	5.6	33	126.0
13	7.5	5.2	5.2	1147	19.89	38.03	4.8	15	40.0
14	7.5	5.2	5.2	1154	29.23	38.03	3.4	11	24.0
15	7.5	5.2	5.2	1159	21.77	38.03	4.3	14	35.0
16	7.5	5.2	5.2	1156	19.29	38.03	5.0	17	42.0
17	7.5	5.2	5.2	1104	13.29	38.03	2.3	10	18.0
18	7.5	5.2	5.2	1081	20.21	38.03	2.9	11	17.0
19	7.5	5.2	5.2	1163	18.77	38.03	4.3	13	22.0
20	7.5	5.2	5.2	1105	32.17	38.03	4.3	25	92.0
21	7.5	5.2	5.2	1140	20.78	38.03	2.0	10	17.0

of hydrogen on the α-to-β phase transition temperatures for zirconium alloys; see [41, 42] and references therein.

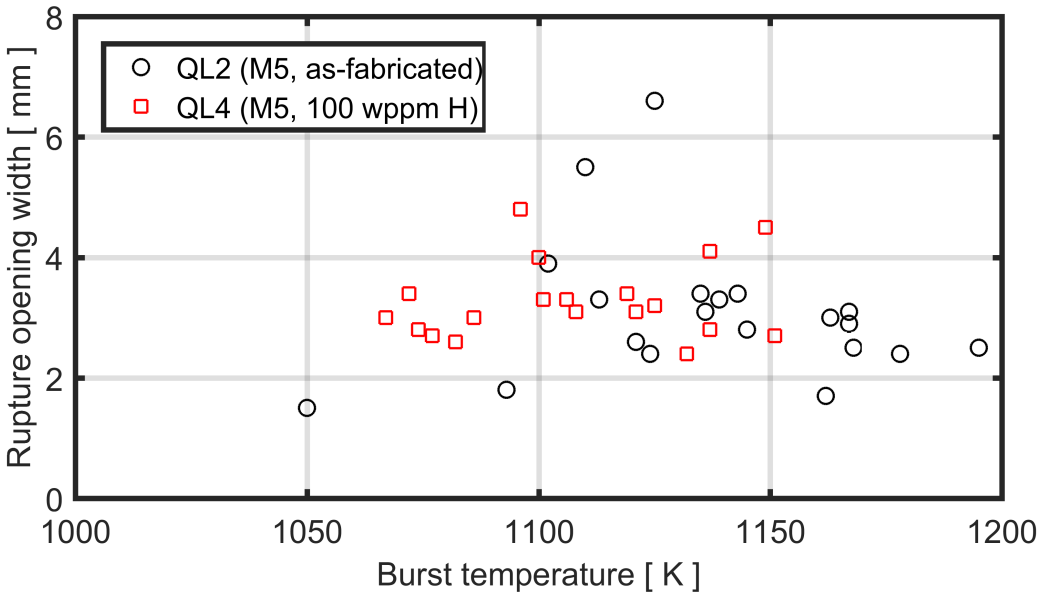

Figure A.21: Measured rupture opening width, w_b, versus burst temperature, T_b, for M5 cladding in as-fabricated and hydrogen-charged condition.

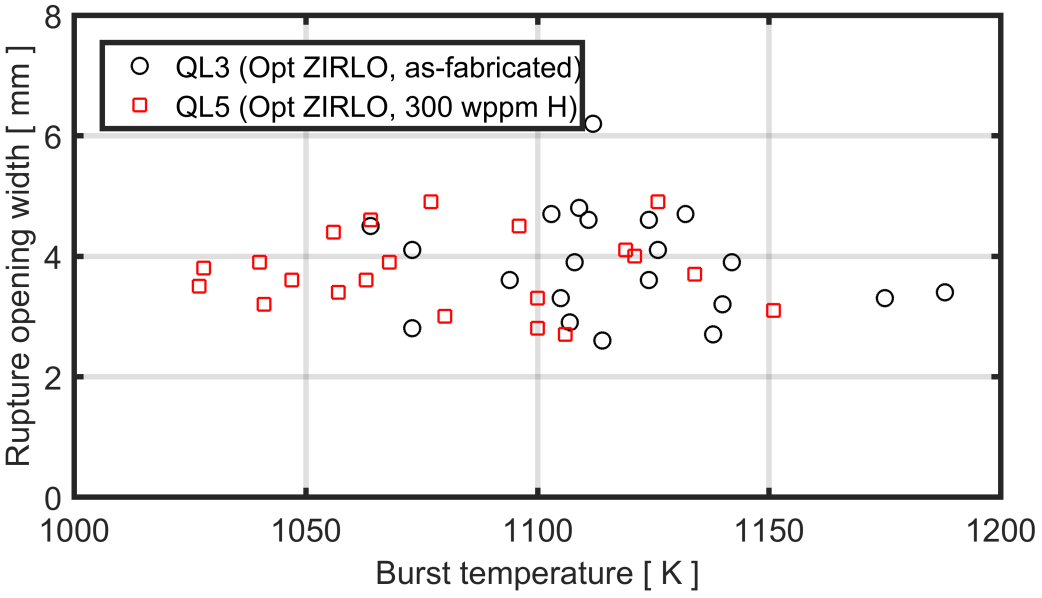

Figure A.22: Measured rupture opening width, w_b, versus burst temperature, T_b, for Optimized ZIRLO cladding in as-fabricated and hydrogen-charged condition.

Table A.12: Data from the QL2 experiment on fuel rods with as-fabricated M5 cladding [28].

Test rod	$\dot{T}$ [Ks^{-1}]	ΔP_o [MPa]	ΔP_b [MPa]	T_b [K]	ε_b [%]	σ_b [MPa]	w_b [mm]	l_b [mm]	A_b [mm^2]
1	7.5	5.2	5.2	1135	11.93	38.03	3.4	14.0	29
2	7.5	5.2	5.2	1167	11.41	38.03	2.9	11.0	20
3	7.5	5.2	5.2	1168	12.10	38.03	2.5	10.0	15
4	7.5	5.2	5.2	1167	12.41	38.03	2.9	11.5	21
5	7.5	5.2	5.2	1163	14.82	38.03	3.0	11.5	21
6	7.5	5.2	5.2	1121	10.90	38.03	2.6	11.0	17
7	7.5	5.2	5.2	1136	13.22	38.03	3.1	12.0	23
8	7.5	5.2	5.2	1113	9.23	38.03	3.3	12.0	24
9	7.5	5.2	5.2	1162	10.37	38.03	1.7	11.0	12
10	7.5	5.2	5.2	1125	9.76	38.03	6.6	22.0	85
11	7.5	5.2	5.2	1145	12.11	38.03	2.8	12.0	21
12	7.5	5.2	5.2	1195	11.10	38.03	2.5	11.0	19
13	7.5	5.2	5.2	1178	12.29	38.03	2.4	10.0	15
14	7.5	5.2	5.2	1167	12.12	38.03	3.1	12.0	23
15	7.5	5.2	5.2	1124	15.19	38.03	2.4	13.0	25
16	7.5	5.2	5.2	1143	10.43	38.03	3.4	13.0	27
17	7.5	5.2	5.2	1102	6.35	38.03	3.9	20.0	66
18	7.5	5.2	5.2	1139	14.23	38.03	3.3	12.0	24
19	7.5	5.2	5.2	1093	13.07	38.03	1.8	11.0	12
20	7.5	5.2	5.2	1110	5.81	38.03	5.5	24.0	94
21	7.5	5.2	5.2	1050	7.16	38.03	1.5	15.0	16

Table A.13: Data from the QL3 experiment on fuel rods with as-fabricated Optimized ZIRLO cladding [29].

Test rod	$\dot{T}$ [Ks^{-1}]	ΔP_o [MPa]	ΔP_b [MPa]	T_b [K]	ε_b [%]	σ_b [MPa]	w_b [mm]	l_b [mm]	A_b [mm^2]
1	7.5	5.2	5.2	1103	12.08	38.03	4.7	16.0	36
2	7.5	5.2	5.2	1140	15.52	38.03	3.2	11.5	21
3	7.5	5.2	5.2	1111	17.38	38.03	4.6	15.0	37
4	7.5	5.2	5.2	1108	18.45	38.03	3.9	12.0	26
5	7.5	5.2	5.2	1109	13.59	38.03	4.8	18.0	44
6	7.5	5.2	5.2	1112	18.44	38.03	6.2	20.0	67
7	7.5	5.2	5.2	1124	14.98	38.03	4.6	14.0	36
8	7.5	5.2	5.2	1107	12.41	38.03	2.9	12.0	20
9	7.5	5.2	5.2	1132	16.28	38.03	4.7	16.0	43
10	7.5	5.2	5.2	1188	13.13	38.03	3.4	13.0	24
11	7.5	5.2	5.2	1126	15.66	38.03	4.1	14.5	33
12	7.5	5.2	5.2	1175	12.93	38.03	3.3	14.0	24
13	7.5	5.2	5.2	1138	12.41	38.03	2.7	12.0	18
14	7.5	5.2	5.2	1124	13.24	38.03	3.6	15.0	27
15	7.5	5.2	5.2	1105	12.93	38.03	3.3	13.5	24
16	7.5	5.2	5.2	1142	12.15	38.03	3.9	15.0	29
17	7.5	5.2	5.2	1094	12.84	38.03	3.6	14.0	28
18	7.5	5.2	5.2	1114	12.30	38.03	2.6	12.5	17
19	7.5	5.2	5.2	1073	13.11	38.03	2.8	12.0	18
20	7.5	5.2	5.2	1064	8.77	38.03	4.5	15.5	39
21	7.5	5.2	5.2	1073	15.36	38.03	4.1	17.5	40

Table A.14: Data from the QL4 experiment on fuel rods with M5 cladding charged with 100 wppm hydrogen [30].

Test rod	$\dot{T}$ [Ks^{-1}]	ΔP_o [MPa]	ΔP_b [MPa]	T_b [K]	ε_b [%]	σ_b [MPa]	w_b [mm]	l_b [mm]	A_b [mm^2]
1	7.5	5.2	5.2	1086	12.12	38.03	3.0	11	20
2	7.5	5.2	5.2	1121	12.32	38.03	3.1	12	21
3	7.5	5.2	5.2	1106	11.23	38.03	3.3	13	25
5	7.5	5.2	5.2	1101	13.23	38.03	3.3	12	24
6	7.5	5.2	5.2	1108	12.52	38.03	3.1	11	20
7	7.5	5.2	5.2	1100	10.56	38.03	4.0	16	34
8	7.5	5.2	5.2	1125	13.52	38.03	3.2	12	21
9	7.5	5.2	5.2	1119	13.73	38.03	3.4	13	26
10	7.5	5.2	5.2	1072	9.93	38.03	3.4	16	26
11	7.5	5.2	5.2	1067	10.02	38.03	3.0	12	20
12	7.5	5.2	5.2	1132	10.49	38.03	2.4	12	16
13	7.5	5.2	5.2	1151	10.41	38.03	2.7	12	18
14	7.5	5.2	5.2	1149	10.17	38.03	4.5	18	40
15	7.5	5.2	5.2	1074	9.21	38.03	2.8	13	18
16	7.5	5.2	5.2	1137	11.31	38.03	2.8	13	20
18	7.5	5.2	5.2	1137	15.36	38.03	4.1	14	34
19	7.5	5.2	5.2	1082	11.40	38.03	2.6	11	17
20	7.5	5.2	5.2	1096	15.69	38.03	4.8	16	39
21	7.5	5.2	5.2	1077	10.61	38.03	2.7	12	19

Table A.15: Data from the QL5 experiment on fuel rods with Optimized ZIRLO cladding charged with 300 wppm hydrogen [31].

Test rod	$\dot{T}$ [Ks^{-1}]	ΔP_o [MPa]	ΔP_b [MPa]	T_b [K]	ε_b [%]	σ_b [MPa]	w_b [mm]	l_b [mm]	A_b [mm^2]
1	7.5	5.2	5.2	1057	12.93	38.03	3.4	12.0	24
2	7.5	5.2	5.2	1056	15.97	38.03	4.4	15.5	35
3	7.5	5.2	5.2	1100	13.23	38.03	3.3	13.0	23
4	7.5	5.2	5.2	1068	13.45	38.03	3.9	14.5	29
5	7.5	5.2	5.2	1080	13.12	38.03	3.0	13.0	21
6	7.5	5.2	5.2	1063	13.34	38.03	3.6	14.0	27
7	7.5	5.2	5.2	1077	17.49	38.03	4.9	17.5	46
8	7.5	5.2	5.2	1041	14.52	38.03	3.2	13.0	21
9	7.5	5.2	5.2	1040	17.45	38.03	3.9	13.5	28
10	7.5	5.2	5.2	1121	16.15	38.03	4.0	14.0	31
11	7.5	5.2	5.2	1134	14.04	38.03	3.7	14.0	27
12	7.5	5.2	5.2	1126	16.49	38.03	4.9	18.0	52
13	7.5	5.2	5.2	1106	13.00	38.03	2.7	13.0	19
14	7.5	5.2	5.2	1100	13.71	38.03	2.8	13.0	20
15	7.5	5.2	5.2	1064	10.38	38.03	4.6	18.0	40
16	7.5	5.2	5.2	1151	14.82	38.03	3.1	14.0	24
17	7.5	5.2	5.2	1096	14.67	38.03	4.5	16.0	41
18	7.5	5.2	5.2	1119	17.86	38.03	4.1	14.5	34
19	7.5	5.2	5.2	1027	15.64	38.03	3.5	14.5	29
20	7.5	5.2	5.2	1047	16.34	38.03	3.6	14.0	29
21	7.5	5.2	5.2	1028	21.75	38.03	3.8	12.0	28

The Swedish Radiation Safety Authority has a comprehensive responsibility to ensure that society is safe from the effects of radiation. The Authority works from the effects of radiation. The Authority works to achieve radiation safety in a number of areas: nuclear power, medical care as well as commercial products and services. The Authority also works to achieve protection from natural radiation an to increase the level of ratiation safety internationally.

The Swedish Radiation Safety Authority works proactively and presentively to protect people and the environment from the harmful effects of radiation, now and in the future.
The Authority issues regulations and supervises compliance, while also supporting research, providing training and information, and issuing advice. Often, activities involving radiation require licences issued by the Authority. The Swedish Radiation Safety Authority maintains emergency preparedness around the clock with the aim of limiting the aftermath of radiation accidents and the unintentional spreading of radioactive substances. The Authority participates in international co-operation in order to promote radiation safety and finances projects aiming to raise the level of radiation safety in certain Eastern European countries.

The Authority reports to the Ministry of the Environment and has around 300 employees with competencies in the fields of engineering, natural and behavioral sciences, law, economics and communications. We have recieved quality, environmental and working environment certification.

Publikationer utgivna av Strålsäkerhetsmyndigheten kan laddas ned via stralsäkerhetsmyndigheten.se eller beställas genom att skicka e-post till registrator@ssm.se om du vill ha broschyren i alternativt format, som punktskrift eller daisy.

Strålsäkerhetsmyndigheten
Swedish Radiation Safety Authority
SE-171 16 Stockholm
Phone: 08-799 40 00
Web: ssm.se
E-mail: registrator@ssm.se

E-print AB, 2021